EBioMedicine 12 (2016) 280–294

Contents lists available at ScienceDirect

EBioMedicine

journal homepage: www.ebiomedicine.com

Research Paper

Defective Connective Tissue Remodeling in Smad3 Mice Leads to Accelerated Aneurysmal Growth Through Disturbed Downstream TGF-β Signaling

I. van der Pluijm, PhD [a,b,c], N. van Vliet, BSc [b], J.H. von der Thusen, PhD [d], J.L. Robertus, PhD [d], Y. Ridwan, BSc [b], P.M. van Heijningen, BSc [b,c], B.S. van Thiel, MSc [a,b,e], M. Vermeij, BSc [b], S.E. Hoeks, PhD [f], R.M.G.B. Buijs-Offerman, PhD [c], H.J.M. Verhagen, MD, PhD [a], R. Kanaar, PhD [b,g], A.M. Bertoli-Avella, MD, PhD [c,1], J. Essers, PhD [a,b,g,*]

[a] Department of Vascular Surgery, Erasmus University Medical Center, Rotterdam, The Netherlands
[b] Department of Molecular Genetics, Cancer Genomics Netherlands, Erasmus University Medical Center, Rotterdam, The Netherlands
[c] Department of Clinical Genetics, Erasmus University Medical Center, Rotterdam, The Netherlands
[d] Department of Pathology, Erasmus University Medical Center, Rotterdam, The Netherlands
[e] Department of Pharmacology, Erasmus University Medical Center, Rotterdam, The Netherlands
[f] Department of Anesthesiology, Erasmus University Medical Center, Rotterdam, The Netherlands
[g] Department of Radiation Oncology, Erasmus University Medical Center, Rotterdam, The Netherlands

ARTICLE INFO

Article history:
Received 6 June 2016
Received in revised form 29 August 2016
Accepted 8 September 2016
Available online 10 September 2016

Keywords:
Aneurysm
Vascular biology
TGF-β signaling pathway
Echocardiography
Mouse model

ABSTRACT

Aneurysm-osteoarthritis syndrome characterized by unpredictable aortic aneurysm formation, is caused by *SMAD3* mutations. SMAD3 is part of the SMAD2/3/4 transcription factor, essential for TGF-β-activated transcription. Although TGF-β-related gene mutations result in aneurysms, the underlying mechanism is unknown. Here, we examined aneurysm formation and progression in *Smad3*$^{-/-}$ animals.

Smad3$^{-/-}$ animals developed aortic aneurysms rapidly, resulting in premature death. Aortic wall immunohistochemistry showed no increase in extracellular matrix and collagen accumulation, nor loss of vascular smooth muscle cells (VSMCs) but instead revealed medial elastin disruption and adventitial inflammation. Remarkably, matrix metalloproteases (MMPs) were not activated in VSMCs, but rather specifically in inflammatory areas. Although *Smad3*$^{-/-}$ aortas showed increased nuclear pSmad2 and pErk, indicating TGF-β receptor activation, downstream TGF-β-activated target genes were not upregulated. Increased pSmad2 and pErk staining in pre-aneurysmal *Smad3*$^{-/-}$ aortas implied that aortic damage and TGF-β receptor-activated signaling precede aortic inflammation. Finally, impaired downstream TGF-β activated transcription resulted in increased *Smad3*$^{-/-}$ VSMC proliferation.

Smad3 deficiency leads to imbalanced activation of downstream genes, no activation of MMPs in VSMCs, and immune responses resulting in rapid aortic wall dilatation and rupture. Our findings uncover new possibilities for treatment of *SMAD3* patients; instead of targeting TGF-β signaling, immune suppression may be more beneficial.

1. Introduction

Aortic aneurysms significantly increase the risk of tearing (dissection) or rupture of the aorta with life-threatening consequences. As for several cardiovascular diseases, male gender, advanced age, and positive family history are among the main risk factors for developing aneurysms (Albornoz et al., 2006; Grubb and Kron, 2011). Multiple genes for thoracic aortic aneurysms have been identified (Gillis et al., 2013), but most of the underlying genetic and molecular interactions are not known. These genes mainly fall into three categories, based on their function; 1) extracellular matrix integrity and structure, 2) involvement in TGF-β signaling, and 3) cytoskeleton maintenance and mobility. Although their functions are quite different, defects in these genes all lead to aneurysm formation.

The extracellular matrix (ECM) is important for the integrity of the aortic wall and mutations in ECM genes such as Fibulin-4 and Fibrillin-1 hence lead to aneurysm formation. Genetic studies in

Abbreviations: AOS, aneurysm-osteoarthritis syndrome; CTGF, connective tissue growth factor; ECM, extracellular matrix; MFS, Marfan's syndrome; MMP, matrix metalloproteases; TGF-β, transforming growth factor β; VSMC, vascular smooth muscle cell; LDS, Loeys-Dietz syndrome; SMAD, SMA/MAD homologous.

* Corresponding author at: Erasmus MC Room Ee702, Wytemaweg 80, 3015 CN Rotterdam, The Netherlands.
E-mail address: j.essers@erasmusmc.nl (J. Essers).
[1] Present address: Centogene AG, Rostock, Germany.

http://dx.doi.org/10.1016/j.ebiom.2016.09.006

Fibulin-4 and Fibrillin-1 mutant mice implicated dysregulation of the TGF-β pathway as an important hallmark in the pathogenesis of aneurysm formation, both in mice and humans (Neptune et al., 2003; Habashi et al., 2006; Hanada et al., 2007; Huang et al., 2010; Kaijzel et al., 2010; McLaughlin et al., 2006).

Several genes that are involved in cytoskeletal maintenance are mutated in aneurysmal disease. Examples are ACTA2 and MYH11, which function in the contractile apparatus of the smooth muscle cell, and mainly cause thoracic aneurysms when mutated (Guo et al., 2007; Zhu et al., 2006), underscoring the importance of cytoskeleton maintenance and mobility in aneurysmal disease.

The TGF-β pathway plays a relevant role in the etiology of aortic aneurysms. Twenty years ago, the first member of the TGF-β signaling pathway was linked to a genetic vascular disease, after finding mutations in the gene coding endoglin (McAllister et al., 1994). Loss of function mutations in this TGF-β binding protein were described to cause hereditary hemorrhagic telangiectasia type I. This was followed by the discovery of mutations in the receptors TGFβR1 and TGFβR2 (Loeys et al., 2005; Mizuguchi et al., 2004), SMAD3 (van de Laar et al., 2011), the ligands TGFβ2 (Lindsay et al., 2012; Boileau et al., 2012) and TGFβ3 (Bertoli-Avella et al., 2015; Rienhoff et al., 2013). These mutations lead to a spectrum of systemic disorders characterized by aneurysms and other cardiovascular and skeletal features known as Loeys-Dietz syndrome (LDS).

The SMAD (SMA/MAD homology) proteins are important regulators of the TGF-β signaling pathway and function as signaling transducers downstream of TGF-β receptors. The SMAD protein family consists of receptor SMADs (SMAD1–3, SMAD5, SMAD8), the co-effector SMAD4 and inhibitory SMADs (SMAD6 and SMAD7) (Massague, 2012; Massague et al., 2005). Activated SMAD2 and SMAD3 can form heteromeric (pSMAD2/4, pSMAD3/4) complexes in the nucleus where they form transcription-activating complexes capable of inducing or repressing the expression of several genes (Massague et al., 2005; Moustakas and Heldin, 2002) in a cell-type and SMAD complex-dependent manner.

We recently described a genetic disease characterized by aneurysms, dissections and cardiac abnormalities in combination with early-onset osteoarthritis (OA) known as aneurysm-osteoarthritis syndrome (AOS or LDS3; MIM 613795) caused by heterozygous mutations in the *SMAD3* gene (van de Laar et al., 2011). Patients carrying heterozygous *SMAD3* mutations present with extreme clinical variability in cardiovascular disease onset and progression (van de Laar et al., 2012; van der Linde et al., 2012; van der Linde et al., 2013). The exact molecular mechanisms and contributing factors underlying this lack of genotype-phenotype correlation remain to be established, as well as the variable effect that genetic variants of *SMAD3* can have on different tissues. *SMAD3* mutations are suggested to lead to upregulation of the TGF-β pathway in the aortic wall as indicated by nuclear translocated and activated SMAD2 (pSMAD2) (van de Laar et al., 2011). Activated SMAD2 is also seen upon mutational hits in the TGFβR1/2 receptors, or the TGFβ2 ligand (Lindsay and Dietz, 2011; Lindsay et al., 2012; Loeys et al., 2005). Because pSMAD2 is considered to report on activation of the TGFβ pathway, these finding are referred to as the TGFβ paradox, as one would expect that mutations in genes involved the TGFβ pathway would hamper TGFβ signaling (Akhurst, 2012; Massague, 2012). However, it is unclear whether pSMAD2 is a functional marker for the downstream upregulation of the TGFβ pathway. Similarly, mutations in genes involved in build-up and integrity of the ECM lead to an upregulation of the TGF-β signaling pathway and aneurysm formation. For the ECM related gene mutations it is thought that this upregulation is due to release of TGF-β ligand from the ECM, caused by loss of ECM integrity, resulting in ECM remodeling and aortic stiffness (Gillis et al., 2013). It remains to be seen whether the same underlying mechanism is at work when comparing ECM- and TGF-β related gene deficiency in aneurysm formation.

The clinical heterogeneity in AOS patients makes it difficult to study *SMAD3* mutational effects on aneurysm formation. Fortunately, due to the homogenous genetic background, genetically engineered mouse models are useful in pinpointing the specific molecular mechanism leading to disease. *Smad3* knockout animals present with skeletal abnormalities and osteoarthritis (OA) and as such, they have been used as a model to study OA (Yang and Cao, 2001; Li et al., 2009). A cardiovascular phenotype in these animals was overlooked until the recent link of human *SMAD3* mutations and aortic aneurysms was established (Regalado et al., 2011; van de Laar et al., 2011; Ye et al., 2013). Here we describe the cardiovascular phenotype of the *Smad3* knockout mice and reveal the underlying mechanism of aneurysm growth caused by a SMAD3 deficiency.

2. Materials and Methods

2.1. Experimental Animals

Smad3$^{+/-}$ animals were bred into in a C57BL6 background to obtain *Smad3*$^{-/-}$ and *Smad3*$^{+/+}$ experimental animals (backcross 6). The numbers of animals, as well as procedures used, are described in the results section and below, respectively. Animals were housed at the Animal Resource Centre (Erasmus University Medical Centre), which operates in compliance with the "Animal Welfare Act" of the Dutch government, using the "Guide for the Care and Use of Laboratory Animals" as its standard. As required by Dutch law, formal permission to generate and use genetically modified animals was obtained from the responsible local and national authorities. An independent Animal Ethics Committee of the Erasmus Medical Center (Stichting DEC Consult) approved these studies (permit number 140–12-05), in accordance with national and international guidelines.

Litter- and gender matched controls were used for each experiment when available.

2.2. Echocardiographic Measurements

Ascending aortic diameter was measured in M-mode, aortic root diameter was measured at the site of the sinus of Valsalva in B-mode. Aortic length was measured as the distance between the sinus of Valsalva and the brachiocephalic trunk. All mice were ventilated and anesthetized with 2.5% isoflurane and echocardiography of the ascending aorta was performed using a Vevo2100 (VisualSonics Inc., Toronto, Canada). Longitudinal echocardiographic measurements of the ascending aorta were performed on 6, 12, 18 and 26 week old *Smad3*$^{-/-}$ and *Smad3*$^{+/+}$ mice ($n = 18$, 8 male and 10 female per genotype).

2.3. Immunohistochemistry

For histological analysis mice were euthanized by CO_2-inhalation. After opening thorax and abdomen, mice were fixed by perfusion fixation through the left ventricle, with PBS and formalin. Organs were weighed and inspected for macroscopic abnormalities. Organs and tissues were fixed in formalin. Aortas were dehydrated through the histokinette processor (Microm), and paraffin embedded, after which 5-μm sections were prepared. Aortas were stained with HE for general pathology, Resorcin-Fuchsin (RF; Elastin von Gieson) for elastin structure, Alcian Blue (AB) to evaluate the extracellular matrix (ECM), and Picrosirius Red (PR) to assess collagen accumulation.

For immunohistochemical analyses, thoracic aortic sections were boiled in 100 mM Tris-HCl [pH 9.0] with 10 mM EDTA at 300 W for 20 min for antigen exposure, and emerged in 3% H_2O_2 in methanol to inhibit endogenous peroxidase for pSmad2, α-SMA, pERK, CD31, MMP, CD3, MAC2 and Ki-67 staining. Slides were first blocked in 5% Protifar in PBS and 0.025% Triton, and incubated with the primary antibodies

overnight at 4 °C; Anti-Human Smooth Muscle Actin (1:100 mouse, clone 1A4 Dako), pSmad2 (1:100 monoclonal Rabbit *anti*-pSmad2 (S465|467 (138D4) Cell Signaling), pERK (1:200 Rabbit Polyclonal anti-pErk (phosphor-p44/42 Mapk (Erk1/2) (Thr202/Tyr204) antibody) (#9101) Cell Signaling), MMP-9 (1:50 goat polyclonal anti MMP-9 (sc-6840) Santa Cruz Biotechnology, Ki-67 (1:200 Rat anti mouse Ki-67, clone TEC-3, DAKO), MAC-2 (1:500 Rat anti mouse MAC-2, CL8942AP, Cedarlane), CD31 (1:50 Rabbit pAb to CD31, ab28364, Abcam), CD3 (1:200 Polyclonal Rabbit anti human CD3, REF A0452, DAKO). The next day slides were incubated with biotinylated secondary antibodies (1:100 DAKO) and avidin-biotinylated complex (Vectastain Universal Elite ABC kit Vector Laboratories). DAB chromogen (DAKO Liquid Dab substrate-chromogen system) was used as substrate and slides were counterstained with hematoxylin. In total 8 *Smad3*$^{-/-}$ and 8 *Smad3*$^{+/+}$ mice were examined for each staining.

2.4. Molecular Imaging for MMP Activation

We used vascular fluorescent mediated tomography (FMT) imaging with near-infrared fluorescent protease activatable probes as previously described (Kaijzel et al., 2010; Nahrendorf et al., 2011). As in aortic aneurysms MMP2 and MMP9 are most abundant, the probe is mostly cleaved by these two proteases. FMT imaging was performed using an FMT 2500 system (Perkin Elmer, Inc.) at 680/700 nm excitation and emission wavelengths, 24 h after tail vein injection of 2 nmol per 25 g bodyweight of the MMPsense™ 680 probe, or at 750/775 nm excitation and emission wavelengths, 6 h after injection of 2 nmol per 25 g bodyweight of the MMPsense™750 FAST near-infrared fluorescent probe (Perkin Elmer, Inc.), mice were imaged in a portable animal imaging cassette between optically translucent windows. The FMT 2500 quantitative tomography software was then used to calculate 3D fluorochrome concentration distribution of the fluorescent signal. After fluorescence imaging, aortas were harvested and fluorescence was quantified using the FMT 2500 or Odyssey imaging systems (LI-COR Inc.). Near-infrared images were obtained in the 680- and 750-nm channels, respectively. Relative fluorescence intensities were calculated for each *Smad3*$^{-/-}$ animals compared to its *Smad3*$^{+/+}$ littermate control.

2.5. CT-scans

μCT imaging was performed using a Quantum FX μCT system (90 kV,160 μA,FOV 60 mm, 2 min 85 mGy scantime) (Perkin Elmer, Inc.). To visualize the vasculature, blood-pool contrast was administered via tail vein injection with 150 μl eXIA™160 Iodine based Radiocontrast (160 mg I/ml) per 25 g bodyweight (Binitio biomedical). A mouse imaging shuttle device was used to sequentially image the mice with both the FMT 2500 and Quantum FX, achieving accurate animal positioning to align both the fluorescence and μCT images. The optical and CT data sets were co-registered in 3 dimensions using the TrueQuant software (Perkin Elmer, Inc.). This multimodal approach allows simultaneous monitoring of aneurysm growth and MMP- activity.

2.6. Isolation of SMCs, Characterization, Cell Culture and Proliferation Assay

Vascular SMCs were isolated from the media of the aortic arch of *Smad3*$^{-/-}$ and *Smad3*$^{+/+}$ mice. The tissue was washed with PBS, cut into 5 mm pieces with the luminal side on 0.1% gelatin-coated cell culture dishes and incubated. After 7–10 days, smooth muscle-like cell outgrowth was observed. SMCs were maintained in DMEM (Lonza, Leusden, the Netherlands), supplemented with 10% fetal calf serum (HyClone, Thermo Scientific, Breda, the Netherlands), 100 U/ml penicillin and 100 μg/ml streptomycin (Sigma-Aldrich, Zwijndrecht, the Netherlands). For characterization, subconfluent SMCs and HUVECs were grown on coverslips and fixed in 2% paraformaldehyde. Cells were permeabilized with PBS/Triton (0.1%) and blocked with PBS+ (0.5% BSA/0.15% glycine in PBS). Coverslips were incubated overnight with the primary antibody, anti-Human Smooth Muscle Actin (1:1000 mouse, clone 1A4 Dako). After washing, coverslips were incubated with the secondary antibody, alexa fluor 594 goat anti mouse IgG (1:1000, Life technologies). Coverslips were mounted in Vectashield with Dapi (Vector Laboratories). For the proliferation assay, cells were used at passage 5–11. *Smad3*$^{+/+}$ and *Smad3*$^{-/-}$ VSMCs were seeded in triplicate in 6 cm dishes (5000 cells/well) and allowed to attach. The cells were counted with the coulter counter every day for a week.

2.7. RNA Isolation and Real-time PCR

Thoracic (arch and ascending) aortic tissue from *Smad3*$^{+/+}$ and *Smad3*$^{-/-}$ mice, snap frozen and stored at −80 °C, was used for this experiment. RNA was isolated with the RNeasy Fibrous tissue mini kit (Qiagen) for aortic tissue and the RNeasy mini kit (Qiagen) for VSMCs. cDNA was made with the iScript cDNA synthesis kit (Biorad) according to the manufacturer's protocol. Q-PCR was performed with 200 nM forward and reverse primers and iQ™ SYBR® Green Supermix (biorad) on the CFX384 system (Biorad); denaturation at 95 °C for 3 min, 40 cycles denaturation at 95 °C for 15 s, annealing/extension at 55 °C or 60 °C (as indicated below) for 30 s. B2M, Tbp1 and Ppia were used as a housekeeping gene. Relative gene expression levels were determined with the comparative ΔΔCt method. ΔΔCT = (CT(gene of interest, wildtype) − CT(reference gene, wildtype)) − (CT(gene of interest, knock-out) − CT(reference gene, knock-out)), where the fold change is calculated as $2^{\Delta\Delta CT}$.

Primer sequences used for real-time PCR:

	Forward primer	Reverse primer	Size (bp)	Temp (°C)
B2M	5′-CTCACACTGAATTCACCCCCA-3′	5′-GTCTCGATCCCAGTAGACGGT-3′	98	55/60
Tbp1	5′-TCACTCCTGCCACACCAGCTTC-3′	5′-TGACTGCAGCAAATCGCTTGGG-3′	156	60
Ppia	5′-CGCGTCTCCTTCGAGCTGTTTG-3′	5′-TCCGTAGATGGACCTGCCGC-3′	186	60
Ppia	5′-GTCTCCTTCGAGCTGTTTGC-3′	5′-ACCACCCTGGCACATGAATC-3′	138	55
Smad7	5′-CAAACCAACTGCAGGCTGTC-3′	5′-CCCCAGGGGCCAGATAATTC-3′	77	55
Smad6	5′-GCCACTGGATCTGTCCGATT-3′	5′-GGTCGTACACCGCATAGAGG-3′	188	55
Pai-1	5′-TCTTTTTCACATTACAGTGGCCTG-3′	5′-TTTGGGTGACTCTGTTAATTCATC-3′	102	55
Fn1	5′-ACGGACATCTGTGGTGTAGC-3′	5′-CGAGTCTGAACCAAAACCGC-3′	91	55
Timp-1	5′-TCGGACCTGGTCATAAGGGC-3′	5′-GCTTTCCATGACTGGGGTGT-3′	162	55
Ltbp1	5′-CCAAACATGGCAGGCAAGTC-3′	5′-TCCACAGACGTTGATCCCCT-3′	116	55
Tgfb1	5′-GTGGACCGCAACAACGCCATCT-3′	5′-GCAATGGGGGTTCGGGCACT-3′	109	60
Tgfbr1	5′-TCGTCCGCAGCTCCTCATCGT-3′	5′-ACACTGTAATGCCTTCGCCCCC-3′	70	60
Tgfbr2	5′-CGCACGTTCCCAAGTCGGATGT-3′	5′-TCGCTGGCCATGACATCACTGT-3′	118	60

2.8. Western Blotting

Equal amounts of protein (Lowry protein assay) were separated by electrophoresis on a 15% SDS-polyacrylamide gel. Proteins were transferred to a PVDF membrane (Millipore) and blocked with 3% milk powder (ERK, β-catenin) or 5% BSA (pERK) in PBS containing 0.1% Tween-20. Next, blots were incubated overnight with the primary antibody (ERK, 1:2000, Rabbit anti p44/42 MAPK (Erk1/2), #9102S, Cell Signaling, pERK, 1:2000, Rabbit anti Phospho-p44/42 MAPK (Erk1/2) (Thr202/Tyr204), #9101L, Cell Signaling, Mouse anti β-catenin, BD Biosciences (1:5000)). After washing, blots were incubated with HRP-conjugated secondary antibodies. Detection was performed by chemo luminescence. Quantification of protein signals was performed with Fiji. Both Erk as well as pErk levels were corrected for protein content with the loading control β-catenin, after which pErk/Erk levels were calculated.

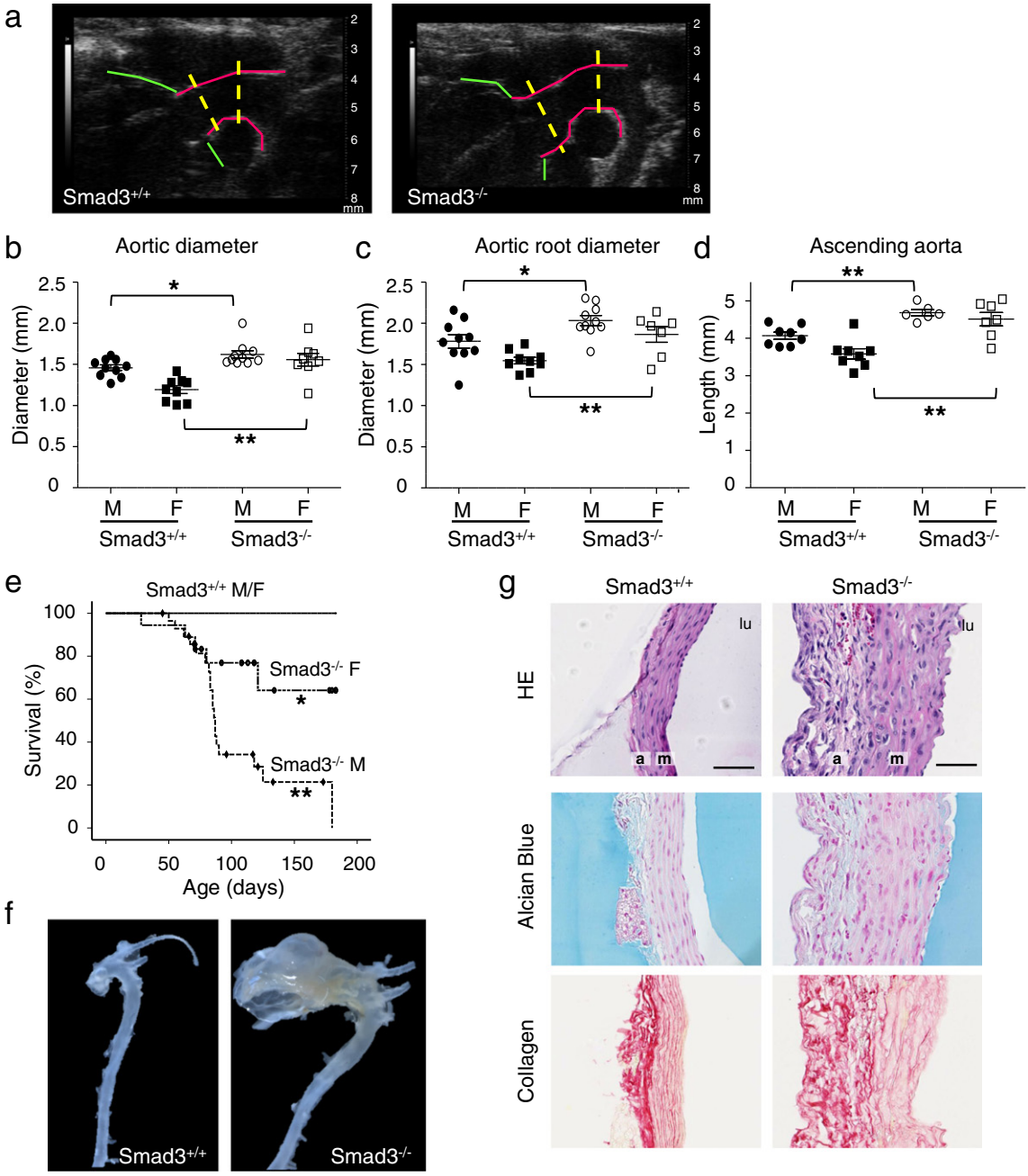

Fig. 1. Increased aneurysm size and early death in *Smad3*$^{-/-}$ mice. a) B-mode ultrasound images of a *Smad3*$^{-/-}$ female mouse and its *Smad3*$^{+/+}$ littermate, age 6 weeks, illustrating aortic diameter measurements. Green line indicates heart, red line the aorta and yellow lines points of measurement. b) Quantification of aortic diameter, c) aortic root and d) aortic length for *Smad3*$^{+/+}$ males (n = 10, 10 and 8 respectively), females (n = 9, 9 and 8 respectively) and *Smad3*$^{-/-}$ males (n = 10, 10 and 6 respectively), females (n = 8, 7 and 7 respectively) at age 6 weeks (*p < 0.05, **p < 0.001, respectively). e) Survival of *Smad3*$^{-/-}$ compared to *Smad3*$^{+/+}$ mice. *Smad3*$^{-/-}$ females (n = 29) and, even more, males (n = 18), show a severely decreased survival (*p < 0.05, **p < 0.001, respectively). f) Representative macroscopic picture of a female *Smad3*$^{-/-}$ (right) and *Smad3*$^{+/+}$ littermate (left) aorta, age 4 months, clearly showing huge dilatation of the *Smad3*$^{-/-}$ thoracic aortic wall, however with the same translucency as its *Smad3*$^{+/+}$ control. g) Representative HE staining (left) of a *Smad3*$^{-/-}$ aorta with aneurysm, age 4 months, showing disruption of the vascular wall, compared to *Smad3*$^{+/+}$ controls. Alcian Blue staining (middle) of *Smad3*$^{-/-}$ aortas showed no increase of ECM in the media compared to *Smad3*$^{+/+}$ aortas. Picrosirius Red staining for collagen deposition in *Smad3*$^{-/-}$ and *Smad3*$^{+/+}$ aortas showed no differences. Observations made for n = 8 per group. Bar = 50 μm, m = media, a = adventitia, lu = lumen.

2.9. TGF-β Transcriptional Response Assay

TGF-β response in VSMCs was determined using the (CAGA)12 — MLP — Luciferase promoter reporter construct (Dennler et al., 1998). This construct contains 12 palindromic repeats of the SMAD3/4 binding element derived from the PAI-1 promoter and was shown to be highly specific and sensitive to TGF-β. The assay was performed as described previously (Hawinkels et al., 2014). In short, VSMCs were seeded in 1% gelatin-coated 24-well plates and allowed to attach overnight. Cells, at subconfluent density, were transfected using Lipofectamine 2000 (Invitrogen, Carlsbad, California, USA) according to the manufacturer's protocol, with the CAGA-luciferase reporter plasmid together with an SV40 renilla-luciferase plasmid to correct for transfection efficiency. After 6 h medium was changed to DMEM containing 10% FCS|PS and the cells were incubated for 24 h. Cells were serum starved overnight after which cells were washed, lysed and luciferase activity was determined with the dual-glo luciferase assay system according to the manufacturer's protocol (Promega). Luciferase activity was corrected for transfection efficiency with renilla activity. The relative increase in luciferase activity was calculated versus controls. Experiments were performed with three independent cell lines, in duplicate.

2.10. Statistical Analysis

For the animal experiments described power analysis was performed with α 0.05 and β 0.80, and taking into account a drop-out rate of 15% due to unforeseen circumstances, which was approved by the local ethical committee. All experiments described were performed blinded by using cell line and mouse numbers without genotypes. Normal distribution of the data was assessed using the Shapiro Wilk test. The unpaired 2-tailed Student *t*-test was performed to analyze the specific sample groups for significant differences. All results are expressed as mean ± SEM. However, for data with non-normal distribution, log-transformation of the data, followed by the Student t-test, was performed. For the differences between genotypes in aortic diameter, aortic root diameter, aortic length and aortic distensibility (Fig. 1b, c and d, S1 Fig. b), Two way ANOVA was performed in order to account for gender effect. Survival curve analysis (Fig. 1e) was performed with the log rank test (with time to death as the outcome). Cell growth curves (Fig. 7c) were fitted to a nonlinear exponential growth equation after which slopes of the curve were compared. A p-value <0.05 was considered to indicate a significant difference between groups. In the figures $p < 0.05$ is shown with *, and $p < 0.01$ with **. All analyses were performed using IBM SPSS Statistics version 21.0 (SPSS Inc., Chicago, IL, USA) and Graphpad.

3. Results

3.1. Increased Aneurysm Size and Early Death in Smad3$^{-/-}$ Mice

In order examine the dynamics of aneurysm formation and progression, we set-up a cross-sectional cohort study of *Smad3*$^{-/-}$ male and female mice together with their *Smad3*$^{+/+}$ littermate controls to perform echocardiograms at 6, 12, 18 and 26 weeks of age. Already at the age of 6 weeks, both *Smad3*$^{-/-}$ male and female mice showed a significant increase in the diameter of the aortic root and ascending aorta compared to their littermate controls. Male *Smad3*$^{-/-}$ mice showed a 14% increase and female *Smad3*$^{-/-}$ mice showed a 21% increase in aortic root diameter (Fig. 1a, b and c, $p < 0.01$). In addition, aortic length, measured from aortic root to the first aortic branch, was significantly increased in *Smad3*$^{-/-}$ mice compared to their wild type littermates; male *Smad3*$^{-/-}$ mice showed a 15% increase and female *Smad3*$^{-/-}$ mice showed a 26% increase in aortic length (Fig. 1d, $p < 0.01$). Interestingly, we observed a correlation between aortic diameter and aortic length increase for *Smad3*$^{-/-}$ animals, indicating that the aorta is enlarged in both dimensions (S1 Fig. a). Strikingly, no significant difference in aortic distensibility was detected in these animals (S1 Fig. b), demonstrating no increase in aortic stiffness. Together these data show limited, though significant dilatations and elongation of *Smad3*$^{-/-}$ aortas at 6 weeks of age.

Smad3$^{-/-}$ mice died suddenly between 6 and 30 weeks of age without overt symptoms, as opposed to none of the *Smad3*$^{+/+}$ mice (Fig. 1e). This effect was even more pronounced in male *Smad3*$^{-/-}$ mice, with 65% mortality for the male animals before 3 months of age (vs. 22% mortality for female mice), implicating a gender difference in life expectancy. Necropsy analysis showed the occurrence of a severe aneurysm consisting of a 2 to 5-fold increase in aortic diameter of the ascending aorta (Fig. 1f). We noticed that the aneurysmatic aortic wall remained translucent, which could be indicative for absence of large-scale ECM remodeling or collagen deposition. HE staining showed altered appearance of smooth muscle cells and apparent changes in aortic wall structure, such as a thicker aortic wall, including a thicker adventitial layer (Fig. 1g). Yet, staining of the aortic wall for Alcian Blue or Picosirius Red showed no differences in proteoglycan and collagen staining, respectively, between *Smad3*$^{-/-}$ and *Smad3*$^{+/+}$ mice (Fig. 1g), which indicates that there is no evidence for increased ECM and collagen accumulation. This is also consistent with the absence of any change in aortic distensibility. Moreover, this is in sharp contrast to what is seen in the *Fibulin4*$^{R/R}$ mouse; in this mouse model, the ECM-involved Fibulin-4 gene is expressed at a 4-fold lower level than wildtype, resulting in stiff aortas that lose their translucency and show increased ECM accumulation and elastin disorganization in the aortic wall (Hanada et al., 2007; Moltzer et al., 2011). To better understand the early and sudden death, we next proceeded with the longitudinal studies at older age to investigate aneurysm formation over time.

3.2. Rapid Aneurysmal Growth in Smad3$^{-/-}$ Mice, Not Restricted to the Aorta

We performed longitudinal ultrasound studies on both female and male *Smad3*$^{-/-}$ mice as well as littermate controls ($n = 8$ and $n = 10$ per group, respectively) with baseline measurements starting at the age of 6 weeks with intervals of 6 weeks. Consistent with aggressive aneurysmal growth in *Smad3*$^{-/-}$ animals, there was a drop-out of 4 females and 7 males during the experiment due to sudden death, which, when possible to determine, all presented with a thoracic aneurysm or a cardiac tamponade (Fig. 2a). Of the surviving *Smad3*$^{-/-}$ animals (4 females and 3 males) 50% of the females and 33% of the males showed a steep increase in aortic diameter in this relative short time span (Fig. 2b and c). No significant increase in aortic diameter was seen in the matched *Smad3*$^{+/+}$ littermate controls in this same time span (data not shown). These data show that *Smad3*$^{-/-}$ animals experience rapid aneurysmal growth, and concurrent early death. Again, this is in contrast to *Fibulin-4*$^{R/R}$ animals that are born with an aneurysm, which shows a slow but progressive growth with age (Te Riet et al., 2016).

To investigate vascular changes throughout the circulatory system we performed μCT-scans with an iodine based contrast agent to visualize soft tissues in *Smad3*$^{-/-}$ and *Smad3*$^{+/+}$ mice ($n = 3$ per genotype). Remarkably, these μCT scans not only revealed a massive dilatation of the aorta and increased heart size, but also enlargements in different locations of the body such as in the jugular vein and the vena cava inferior (Fig. 2d, white, yellow and blue arrows, respectively). However, dilatation of the jugular vein might also be the consequence of cardiac failure. These data indicate that in mice, Smad3-related disease is a widespread and aggressive pathology not restricted to the aorta, similar as previously observed in human (AOS) patients (Aubart et al., 2014; Martens et al., 2013; van de Laar et al., 2012; Regalado et al., 2011). The μCT scans of *Smad3*$^{-/-}$ animals also showed skeletal abnormalities, such as kyphosis, as previously described (Li et al., 2006) and illustrated in our Supporting video files, showing the 3D rotation for both a *Smad3*$^{-/-}$ and *Smad3*$^{+/+}$ mouse (Supporting info files).

a

Smad3$^{-/-}$	Death < 18 wks	Cause		
		Aneurysm	*Cardiac tamponade*	*ND*
Male (n=10)	7	2	3	2
Female (n=8)	4	2	1	1

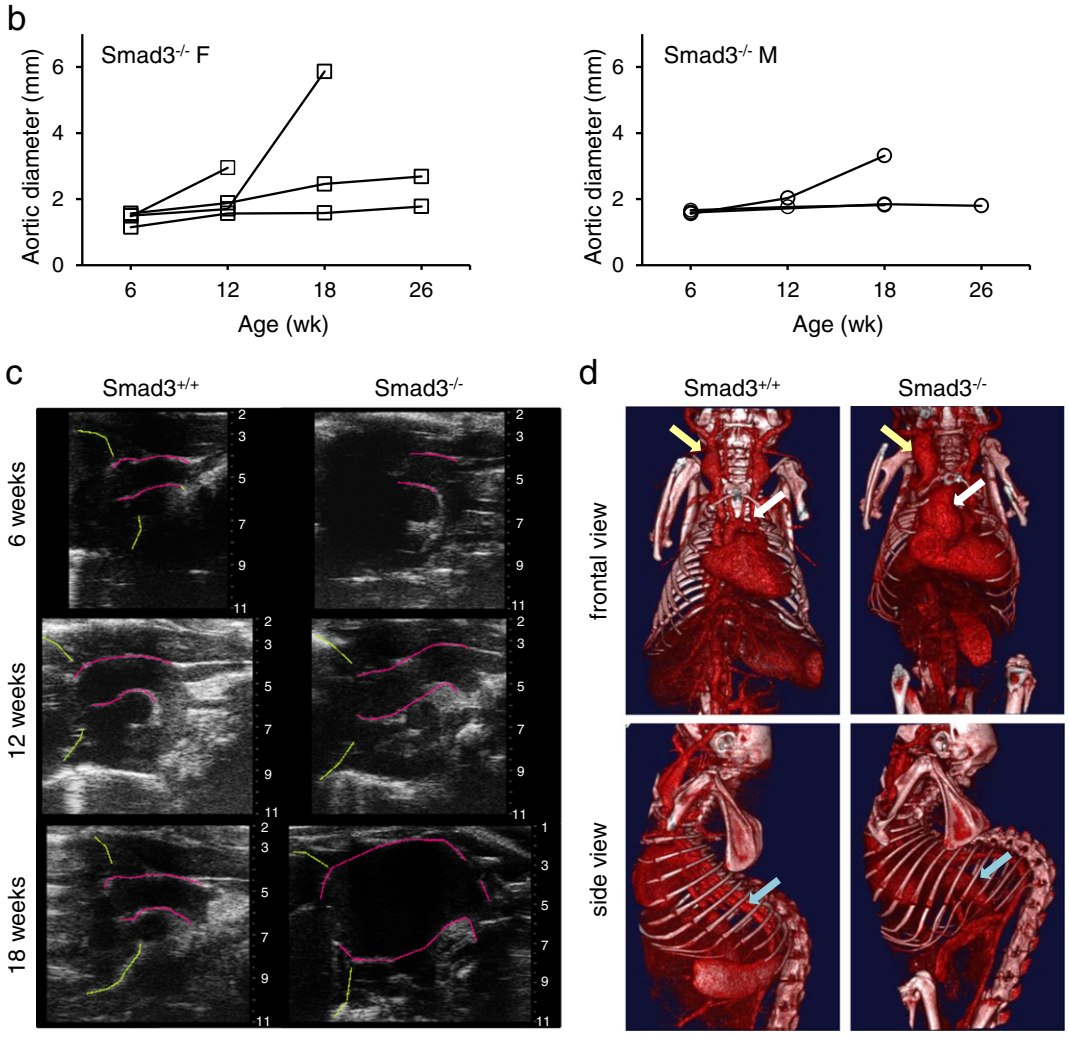

Fig. 2. Rapid aneurysmal growth in *Smad3*$^{-/-}$ mice, not restricted to the aorta. a) Table depicting the fate of *Smad3*$^{-/-}$ mice before 18 weeks, and the possible cause (ND: not determined). b) Graphs depicting aortic diameter in time for *Smad3*$^{-/-}$ females (left, n = 4) and *Smad3*$^{-/-}$ males (right, n = 3). c) B-mode ultrasound images of a *Smad3*$^{-/-}$ female mouse and its littermate, illustrating the huge increase in aortic diameter within 12 weeks of time. Green line indicates heart, red line the aorta. d) Representative CT pictures of a *Smad3*$^{-/-}$ female (right) and its *Smad3*$^{+/+}$ littermate (left), age 4 months, in frontal and side view. Arrows indicate the aortic aneurysm in frontal view (white), enlargement of the jugular vein (yellow), and vena cava inferior (blue), for the *Smad3*$^{-/-}$ mouse. Same sites are indicated in the *Smad3*$^{+/+}$ animal. Bone abnormalities such as kyphosis are also apparent in the *Smad3*$^{-/-}$ mouse.

3.3. Smad3$^{-/-}$ *Aortic Aneurysms Show Elastin Disruption, and Increased Immune Response, pSmad2 and pErk*

Histomorphological analysis of five *Smad3*$^{-/-}$ aortic walls with aneurysms showed changes predominantly in the ascending aorta, consisting of focal disruption and thinning of the media (Fig. 3a). Three aortas with aneurysms showed marked cystic spaces in the medial wall (Fig. 3a), some of which contained erythrocytes, which was not seen in *Smad3*$^{+/+}$ mice (data not shown). We stained for CD31, an endothelial marker, that aligns the endothelial wall of vessels (indicated with an arrow in Fig. 3a and b), demonstrating that these cystic spaces actually represented small capillaries in the adventitia of *Smad3*$^{-/-}$ aortic walls. Occurrence of these capillaries could indicate (neo) vasculogenesis, possibly as a response to vascular damage (Fig. 3b). In line with this observation, disruption of the media structure was seen in conjunction with focal adventitial inflammation, fibrosis and granulation tissue (Fig. 3a). Interestingly, immune infiltrations have not been observed in *Fibulin-4*$^{R/R}$ animals.

Elastin staining clearly showed disruption in the elastin structure of the aortic wall (Fig. 3c). Strikingly, this differs from *Fibulin-4*$^{R/R}$ aortic walls, where accumulation and disorganization of elastin structure was observed (Hanada et al., 2007; Moltzer et al., 2011). At sites where the media was still present, SMA staining did not show apparent loss of VSMCs in *Smad3*$^{-/-}$ aortic walls (Fig. 3d). To investigate the impact of Smad3 deficiency on the TGF-β signaling pathway, we performed pSmad2 and pErk immunohistochemical staining on *Smad3*$^{-/-}$ and

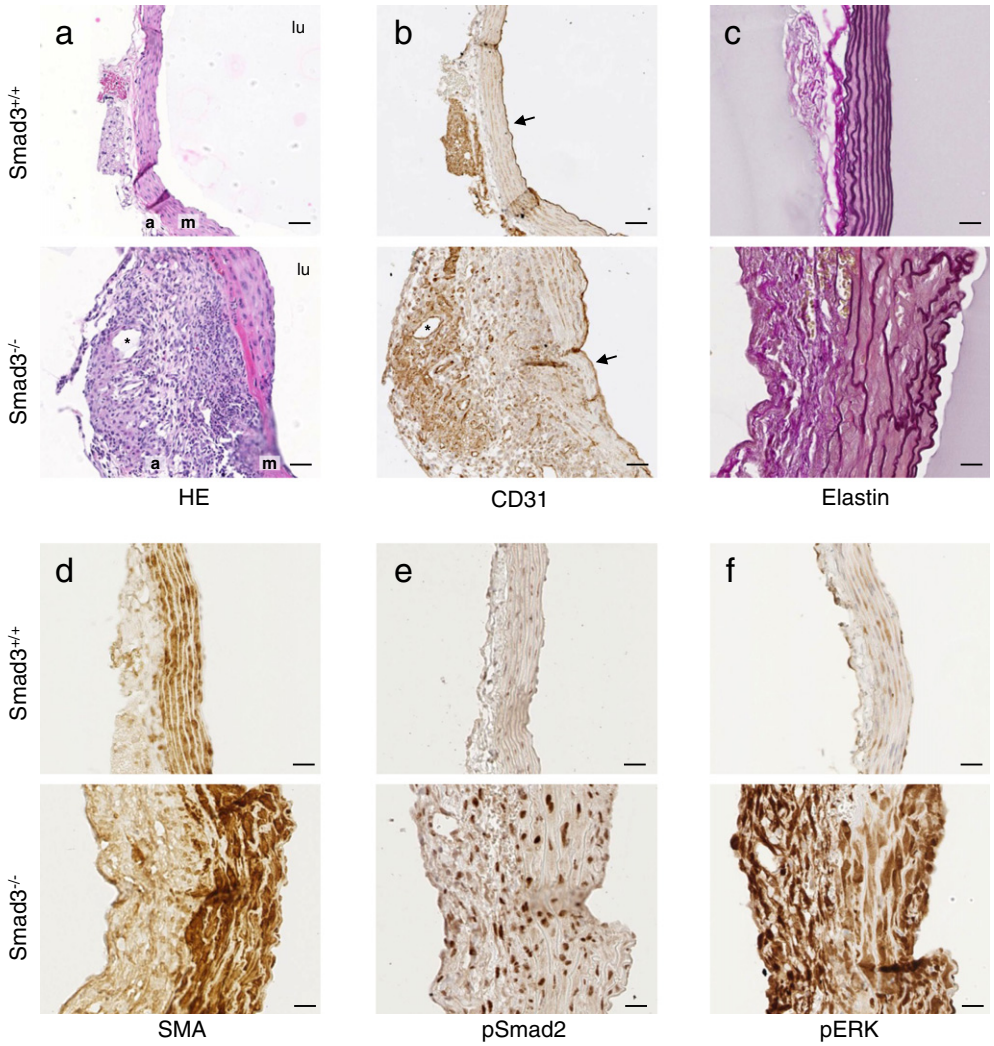

Fig. 3. Aneurysmal *Smad3*$^{-/-}$ aortas show an increased immune response, elastin disruption, pSmad2 and pErk activation. a) HE staining of a *Smad3*$^{-/-}$ aorta with aneurysm showing disruption of the vascular wall, adventitial inflammation, and cystic spaces (example indicated with *). b) CD31 staining shows the endothelial layer (indicated by arrow), but also alignment of the observed cystic spaces (example indicated with *), showing that these spaces represent vessels in the adventitia. c) Resorcin Fuchsin staining for elastin showed disrupted elastin structures in the medial layer in aneurysmal *Smad3*$^{-/-}$ compared to *Smad3*$^{+/+}$ aortas. d) Smooth Muscle Actin staining of aneurysmal *Smad3*$^{-/-}$ aortic walls showed no apparent loss of VSMCs in the media comparable to *Smad3*$^{+/+}$. e) pSmad2 and f) pErk showed increased staining in the aortic wall of aneurysmal *Smad3*$^{-/-}$ compared to *Smad3*$^{+/+}$ mice. This suggests an increased TGF-β receptor activation. Observations made for n = 8 per group, age 3–4 months old. Bar = 50 μm, m = media, a = adventitia, lu = lumen. *; cystic space, arrow; endothelial layer.

Smad3$^{+/+}$ aortic walls. These are markers for canonical (pSmad2) and non-canonical (pErk) activation of the TGF-β signaling pathway via the TGF-β receptor. pSmad2 and pErk are activated in the *Fibulin-4*$^{R/R}$ mouse model, in other aneurysmal diseases such as Marfan's syndrome and other TGF-β pathway related aneurysmal diseases (Hanada et al., 2007; Loeys et al., 2005; Neptune et al., 2003; Renard et al., 2013; Renard et al., 2010). Both pSmad2 as well as pErk staining (Fig. 3e and f), showed an increase in the aorta of *Smad3*$^{-/-}$ animals, indicative of increased TGF-β receptor activation.

3.4. Inflammation-associated MMP Activation in Aneurysmal *Smad3*$^{-/-}$ Mice

An important process that is regulated by the TGF-β signaling pathway is MMP activation. In aneurysmal diseases such as Marfan's syndrome, as well as aneurysmal mouse models, including *Fibulin-4*$^{R/R}$ and Fibrillin-1 mutant mice, MMP activity is strongly increased (Lemaitre et al., 2003; Longo et al., 2002; Segura et al., 1998; Kaijzel et al., 2010; Chung et al., 2007). To examine MMP activation in *Smad3*$^{-/-}$ aortas, we used molecular imaging with MMPsense near-infrared probes to monitor MMP activity both *in vivo* and *ex vivo*. No significant difference in MMP activation between *Smad3*$^{-/-}$ (with no or minor aneurysm formation) and *Smad3*$^{+/+}$ aortas was observed (Fig. 4a, b and c). Thus, also suggesting that an increase in MMP may not always correlate with functional upregulation of the TGF-β signaling pathway. Interestingly, only 25% of aneurysmatic *Smad3*$^{-/-}$ aortas did seem to show an increase in MMP activity (Fig. 4c and d). This is in contrast to *Fibulin-4*$^{R/R}$ animals that show increased MMP activity already at a young age in VSMCs of the aortic wall (Kaijzel et al., 2010). Strikingly, in *Smad3*$^{-/-}$ animals this activation was derived from invading immune cells and not from VSMCs in the medial layer, as evident from immunohistochemical staining for MMP, CD3 (T-cells) and MAC2 (macrophages) (Fig. 4e). Thus, since this MMP activation was not seen in the VSMCs, this indicates impaired TGF-β signaling downstream of Smad3 in VSMCs specifically, leading to a lack of MMP activation and therefore no ECM remodeling. Together with the finding that we do not see changes in ECM composition (staining Fig. 1g), this can explain the fast expansion and rupture of *Smad3*$^{-/-}$ aortas.

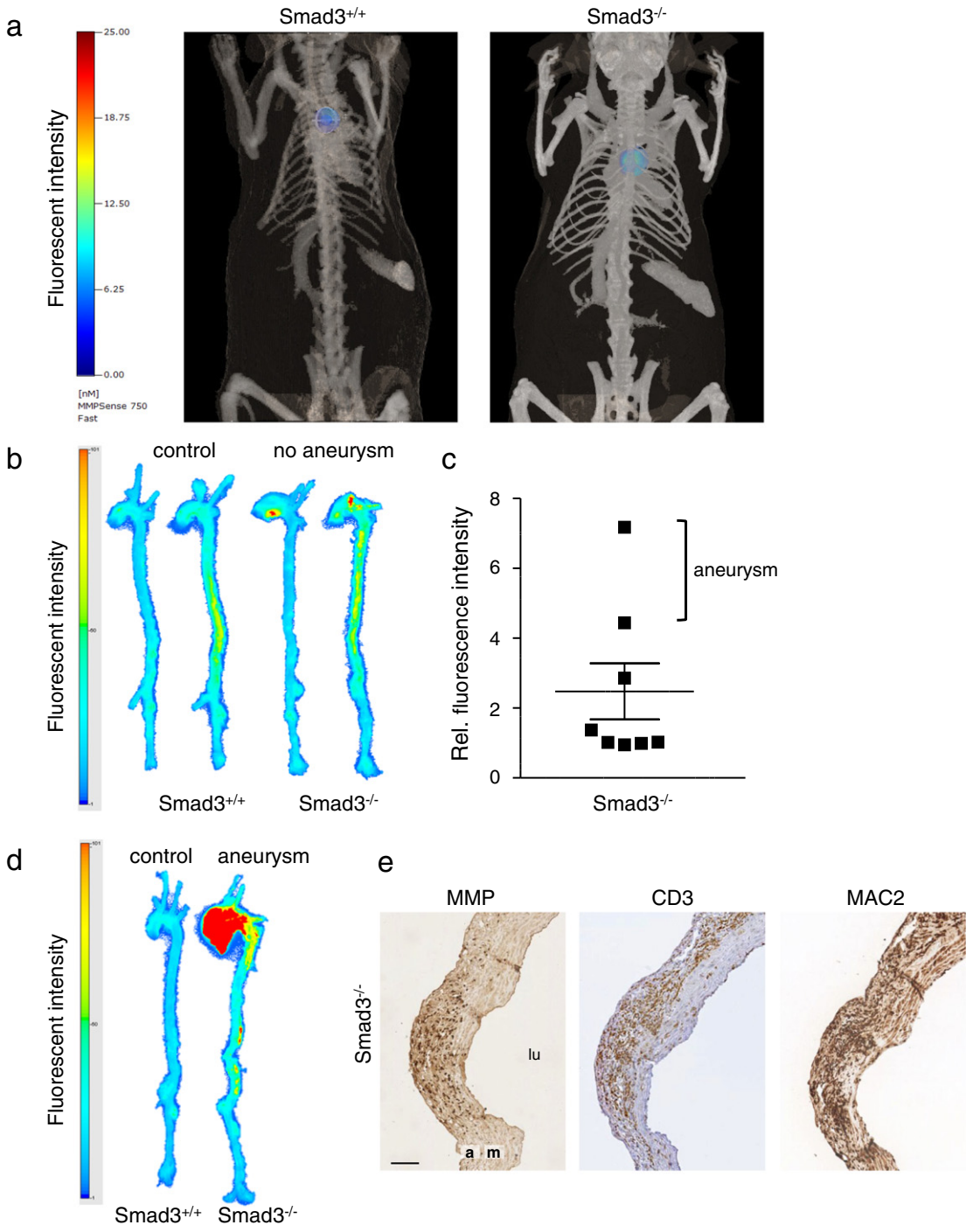

Fig. 4. Inflammation-associated MMP activation in aneurysmal *Smad3*$^{-/-}$ mice. a) Representative *in vivo* images of male *Smad3*$^{-/-}$ and *Smad3*$^{+/+}$ aortas showing comparable MMP activation. b) Representative *ex vivo* images of male *Smad3*$^{-/-}$ and *Smad3*$^{+/+}$ aortas showing similar MMP activation. c) Quantification of the fluorescent signal, a measure for MMP activity, does not show significant differences between *Smad3*$^{-/-}$ and *Smad3*$^{+/+}$ aortas. Values for each *Smad3*$^{-/-}$ aorta are compared to its *Smad3*$^{+/+}$ littermate. Both male and female aortas were used for quantification (n = 8 total). The two *Smad3*$^{-/-}$ aortas with highest relative fluorescence intensity also had an aneurysm. d) Ex vivo images of male *Smad3*$^{-/-}$ aortas with an aneurysm occasionally do show increased MMP activation. e) Immunohistochemical staining for MMP9, T cells (CD3) and macrophages (MAC2) in an aneurysmal *Smad3*$^{-/-}$ aortic wall, showing that the MMP9 signal is derived from immune cells and not VSMCs (performed for n = 5–7 animals per group, age 3–4 months old). bar = 100 μm, m = media, a = adventitia, lu = lumen.

3.5. Pre-aneurysmal Smad3$^{-/-}$ *Animals Show Elastin Disruption and pErk Activation*

As it seemed that specifically *Smad3*$^{-/-}$ aortas with an aneurysm showed increased MMP activity, which might be derived from immune cells infiltrating the aortic wall, we next wondered which histological changes may already occur in pre-aneurysmal *Smad3*$^{-/-}$ animals. HE staining of aortic walls derived from these *Smad3*$^{-/-}$ animals showed morphological changes in VSMC appearance; a more round, less flattened appearance compared to *Smad3*$^{+/+}$ aortas (Fig. 5a). Interestingly, the elastin structure was disrupted at several places in pre-aneurysmal *Smad3*$^{-/-}$ aortic walls, whereas SMA staining at these same sites showed no apparent smooth muscle cell loss (Fig. 5b and c). Surprisingly, pSmad2 and pErk staining were both already increased in the aortas

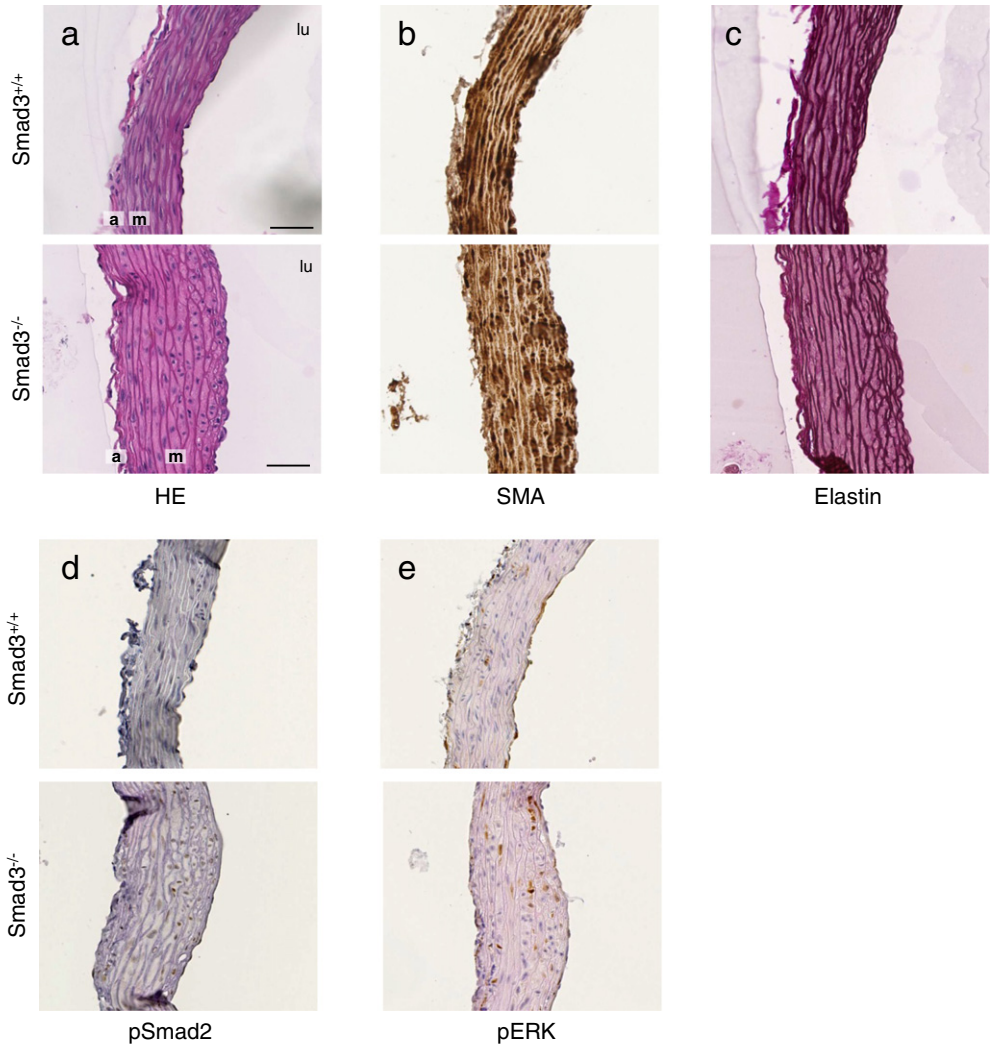

Fig. 5. Pre-aneurysmal *Smad3*$^{-/-}$ animals show elastin disruption, pSmad2 and pErk activation. a) HE staining of pre-aneurysmal *Smad3*$^{-/-}$ aortas showing altered appearance of VSMCs in the medial layer. b) Smooth Muscle Actin staining of pre-aneurysmal *Smad3*$^{-/-}$ aortic walls showed no apparent VSMC loss in the media comparable to *Smad3*$^{+/+}$ aortas. c) Resorcin Fuchsin staining for elastin showed a somewhat disrupted elastin structure in the medial layer of pre-aneurysmal *Smad3*$^{-/-}$ aortas compared to *Smad3*$^{+/+}$. d) pSmad2 staining is already somewhat increased in the aortic wall of pre-aneurysmal *Smad3*$^{-/-}$ compared to *Smad3*$^{+/+}$ mice. e) pErk clearly showed increased staining in the aortic wall of pre-aneurysmal *Smad3*$^{-/-}$ compared to *Smad3*$^{+/+}$ mice. Observations made for n = 5 per group, age 3–4 months old. Bar = 50 μm, m = media, a = adventitia, lu = lumen.

of these pre-aneurysmal *Smad3*$^{-/-}$ animals (Fig. 5d and e), although the increased pErk staining was much more pronounced. However, at these sites of increased structural wall damage and increased pErk staining no apparent immune infiltration was observed (Fig. 5a) In agreement, staining for CD31 and for MAC2 were negative (data not shown). Together this indicates that both the damage in the aortic wall and the canonical and non-canonical TGF-β signaling activation, activated pSmad2, and pErk, precede the structural damage in the medial layers that might trigger the immune response.

3.6. Smad3$^{-/-}$ *VSMCs and Aortas Show No Downstream Transcriptional Activation of TGF-β Signaling*

Although Smad3 is not expressed, we find an increase in nuclear located pSmad2 and pErk activation. As this increased activation normally affects downstream transcriptional activation, as was shown before in *Fibulin-4*$^{R/R}$ aortas (Ramnath et al., 2015), we next decided to investigate the transcription of genes that should normally be activated in response to an increase in TGF-β receptor activation. In particular, next to the aorta itself, we were interested in the transcriptional response in VSMCs isolated from the aorta, as there we can exclude the contribution of other cell types such as immune cells or fibroblasts that are clearly present in the aneurysmal aortas of *Smad3*$^{-/-}$ animals. We therefore isolated VSMCs from *Smad3*$^{-/-}$ and *Smad3*$^{+/+}$ aortas, and confirmed the smooth muscle cell phenotype with SMA staining (Fig. 6a). Next, we determined the mRNA expression levels of FN-1, PAI-1, Smad7 and Smad6 (Fig. 6b–e), together with TIMP-1, LTBP-1, TGFβR1, TGFβR2 and TGFβ1 (S2 Fig. a–e) in aortic extracts as well as in aortic VSMCs of *Smad3*$^{-/-}$ and *Smad3*$^{+/+}$ animals. We found a significant decrease in FN-1, PAI-1 and Smad7 transcription in *Smad3*$^{-/-}$ aortic extracts as well as VSMCs compared to *Smad3*$^{+/+}$ (Fig. 6b and c). Transcription of Smad6 and TIMP-1 was decreased in *Smad3*$^{-/-}$ compared to *Smad3*$^{+/+}$ VSMCs and aortas (Fig. 6d, e and S2 Fig. a), and no significant change in LTBP-1 mRNA levels was detected (S2 Fig. b). Interestingly, transcripts for TGFβR1, TGFβR2 and TGFβ1 were significantly decreased in *Smad3*$^{-/-}$ VSMCs compared to *Smad3*$^{+/+}$, but not in the aortic arch tissue, which could imply that this decrease in TGFβ receptors and TGFβ1 occurs specifically in VSMCs and not in immune (or other types of) cells (S2 Fig. c, d and e). These findings are different from *Fibulin-4*$^{R/R}$ aortas where increased TGFβ receptor activation and downstream transcriptional activation of genes such as TGFβ2 and PAI-1 were observed (Ramnath et al., 2015).

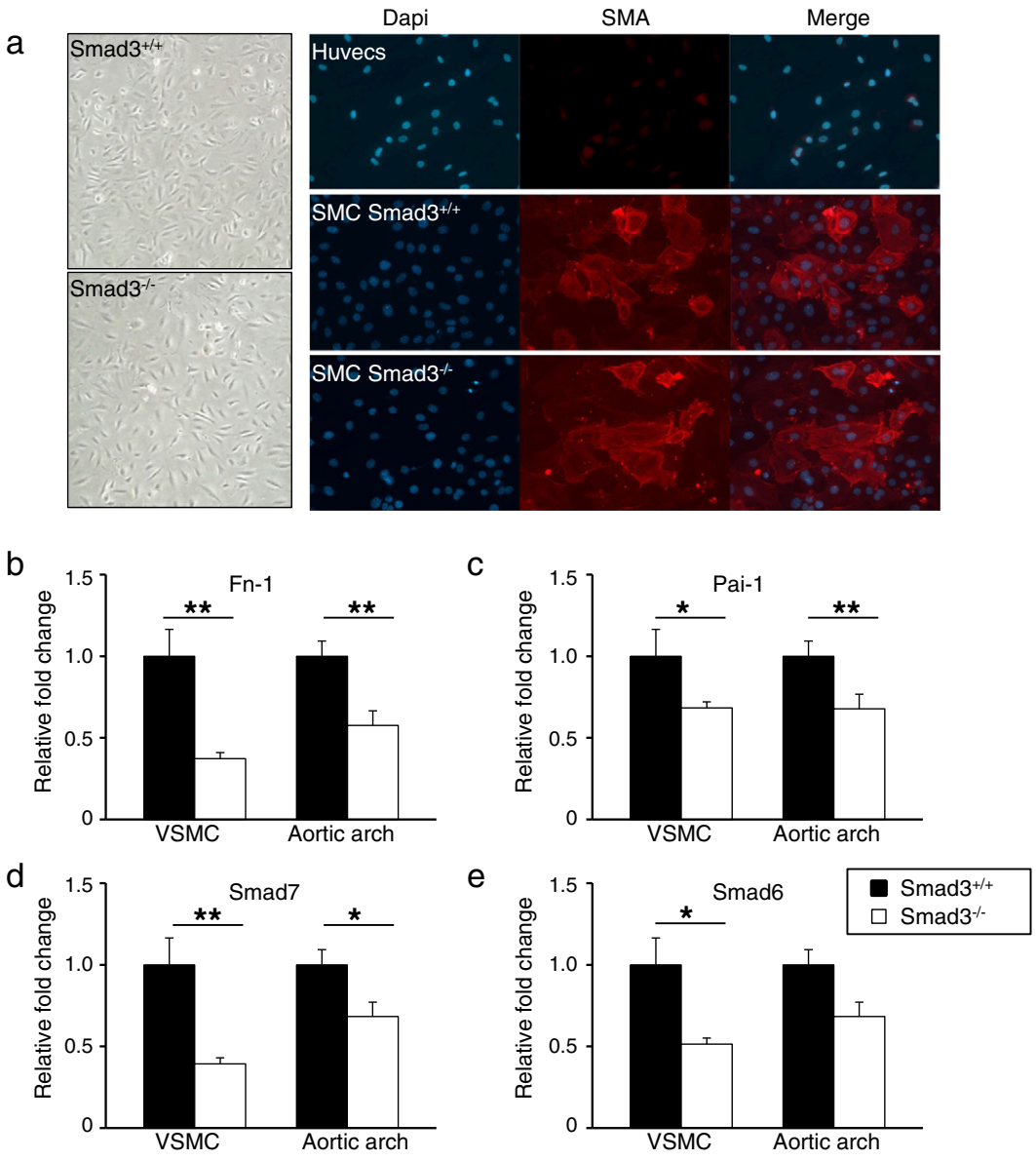

Fig. 6. *Smad3*$^{-/-}$ VSMCs and aortas show no downstream transcriptional activation of TGF-β signaling. a) Pictures showing *Smad3*$^{+/+}$ and *Smad3*$^{-/-}$ VSMCs isolated from the aorta, confirmed by SMA staining. Real-time PCR analysis on VSMC and aorta mRNA shows downregulated mRNA levels of b) Fn-1, c) Pai-1, d) Smad7, and e) Smad6, in *Smad3*$^{-/-}$ VSMCs and aortic extracts compared to *Smad3*$^{+/+}$. Fold changes are shown for *Smad3*$^{-/-}$ relative to *Smad3*$^{+/+}$, *$p < 0.05$, **$p < 0.01$. The mean of three independent experimental means is shown, n = 9–12 per group.

3.7. Increased *Smad3*$^{-/-}$ VSMC Proliferation due to Decreased Downstream Transcriptional Activation

Interestingly, in the *Fibulin-4*$^{R/R}$ mouse model VSMCs have a higher downstream TGF-β-activated transcriptional response, which is linked to their reduced proliferation rate, and which can be rescued by inhibiting TGF-β (Ramnath et al., 2015). In contrast, during the culturing of *Smad3*$^{-/-}$ VSMCs we noticed that they appeared to proliferate faster than *Smad3*$^{+/+}$ VSMCs. We therefore performed Ki67 staining on the aorta, which specifically marks proliferative cells, and found an increase in VSMC proliferation in *Smad3*$^{-/-}$ aortic walls compared to *Smad3*$^{+/+}$ (Fig. 7a) as judged from the positive KI-67 staining. We next set up a controlled VSMC proliferation experiment, where we started with the same amount of cells for each genotype and counted the cells each day for seven days. Indeed, *Smad3*$^{-/-}$ VSMCs proliferated faster than *Smad3*$^{+/+}$ VSMCs (Fig. 7b). This is different from the *Fibulin-4*$^{R/R}$ VSMCs, which proliferate slower than their wild type control cells (Ramnath et al., 2015). As we observed prominent increased pErk staining in both pre-aneurysmal as well as aneurysmal *Smad3*$^{-/-}$ aortas, we next investigated Erk phosphorylation status in both *Smad3*$^{-/-}$ as well as *Fibulin-4*$^{R/R}$ VSMCs. In both *Smad3*$^{-/-}$ and *Fibulin-4*$^{R/R}$ VSMCs pErk was increased compared to their control cell lines (Fig. 7c), which hence does not explain the increased proliferation observed in *Smad3*$^{-/-}$ VSMCs. However, we did observe an impaired downstream TGF-β transcriptional response in *Smad3*$^{-/-}$ VSMCs (Fig. 6). We therefore next decided to measure the transcriptional response in isolated *Smad3*$^{-/-}$ and *Fibulin-4*$^{R/R}$ VSMCs with a luciferase-based reporter assay as previously described (Dennler et al., 1998; Hawinkels et al., 2014; Ramnath et al., 2015). In this assay, a plasmid containing the SMAD3/4 binding element derived from the PAI-1 promoter is transfected, that is highly specific and sensitive to TGF-β receptor activation. We measured the transcriptional response without adding exogenous TGF-β. Although we observed no significant change in transcriptional response for *Fibulin-4*$^{R/R}$ compared to *Fibulin-4*$^{+/+}$ VSMC, *Smad3*$^{-/-}$ VSMCs showed a significantly 5-fold lower response than *Smad3*$^{+/+}$ VSMCs, indicating impaired downstream activation of

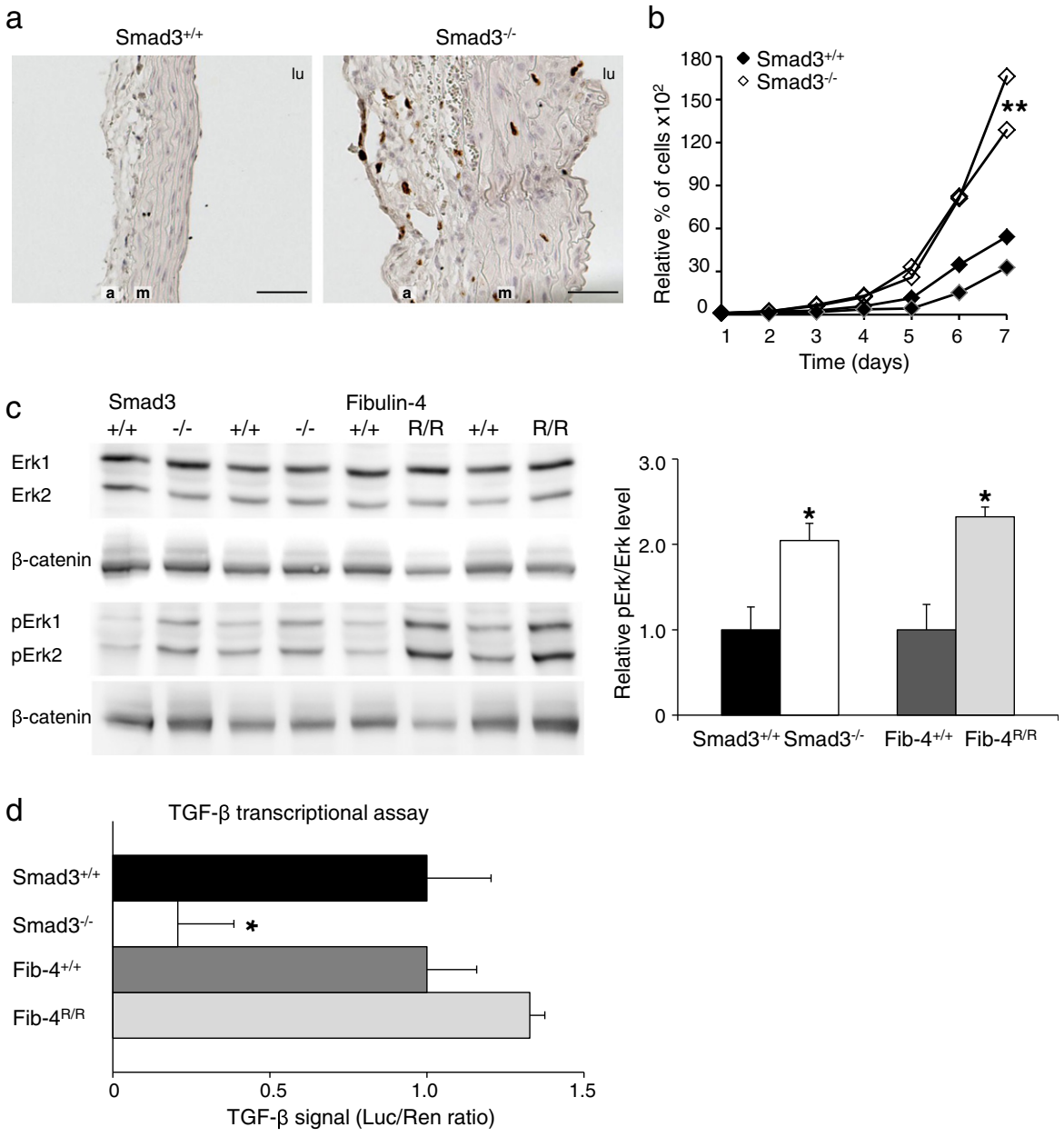

Fig. 7. Increased *Smad3*$^{-/-}$ VSMC proliferation due to decreased TGF-β induced transcriptional activity. a) KI67 staining of *Smad3*$^{-/-}$ aortic walls showing increased proliferation of VSMCs in the medial layer. b) Curve depicting faster growth of *Smad3*$^{-/-}$ VSMCs (open symbols) compared to *Smad3*$^{+/+}$ (closed symbols). On the y-axis, the relative % of cells, compared to the cells at day 1 of the experiment, is shown. c) Western blots for Erk, pErk and loading control β-catenin of *Smad3*$^{-/-}$, *Smad3*$^{+/+}$, *Fibulin-4*$^{+/+}$ and *Fibulin-4*$^{R/R}$ VSMC protein extracts (left). Quantification (corrected for β-catenin levels) shows an increase in pErk/Erk levels in *Smad3*$^{-/-}$ and *Fibulin-4*$^{R/R}$ VSMCs relative to wildtype (right). d) Luciferase TGF-β transcriptional based assay showing a lower transcriptional response in *Smad3*$^{-/-}$ VSMCs relative to *Smad3*$^{+/+}$, and no change in *Fibulin-4*$^{R/R}$ VSMCs compared to *Fibulin-4*$^{+/+}$. Relative luciferase signal compared to wildtype and corrected for transfection efficiency, is shown. Experiment performed with three independent cell lines. Luc = luciferase, Ren = renilla.

TGF-β responsive genes (Fig. 7d, $p < 0.05$). These data imply that the impaired downstream TGF-β induced transcriptional activation affects cellular fate such as proliferation.

4. Discussion

In humans, SMAD3 mutations cause a syndrome with cardiovascular, craniofacial, cutaneous and skeletal anomalies. Aortic aneurysms and osteoarthritis characterize this syndrome known as AOS or LDS3. Although an increasing number of *SMAD3* mutations have recently been reported (Aubart et al., 2014; Fitzgerald et al., 2014; Hilhorst-Hofstee et al., 2013; Zhang et al., 1996), the functional effect of these mutations remains to be explored. The molecular mechanism underlying AOS, resulting from *SMAD3* mutations is largely unknown. In this study we investigated the vascular phenotype in *Smad3* mutant mice and explored its effects on the TGF-β signaling cascade.

As the functional consequence of heterozygous SMAD3 patient mutations at the protein level is unclear; it might for example lead to a null or non-functional protein (e.g. not able to bind SMAD2), we decided to study the effect of *Smad3* deletion in *Smad3*$^{-/-}$ mice to better understand its role in aneurysm formation. In *Smad3*$^{-/-}$ mice, *Smad3* deficiency leads to aortic aneurysms, which mainly affect the aortic root and ascending aorta, but also extends to other major arteries. Aneurysm formation is highly dependent on the age of the animals, as has been observed in AOS patients with *SMAD3* mutations, which display an age-dependent penetrance. As shown here, male *Smad3*$^{-/-}$ animals suffered a more severe aortic phenotype (both dilatation and elongation) and consequently, died earlier than female *Smad3*$^{-/-}$ animals.

The resulting phenotype due to *Smad3* deficiency in mice is very similar to the vascular phenotype described in patients with *SMAD3* mutations offering an excellent opportunity for disease modeling. Despite the homogeneous genetic background aneurysms still present irregularly in the *Smad3*$^{-/-}$ mice, which suggests that other external factors, like for example blood pressure and subtle intrinsic variations in transcriptional activation can also determine the variability in the resulting phenotype.

Strikingly, histology of the aortic wall shows that, unlike other models for aneurysmal disease, there is no increase in ECM accumulation, nor excessive collagen staining, or loss of vascular smooth muscle cells. However, we observe increased aortic pSmad2 and pERK activation. Moreover, this activation is already apparent before Smad3$^{-/-}$ animals present with aneurysms, showing that this activation precedes aneurysm formation. Importantly, these changes in the Smad3$^{-/-}$ aortic wall are distinct from what was previously observed for *Fibulin-4*$^{R/R}$ animals, which have reduced expression of the ECM protein Fibulin-4, and as a result also show aneurysm formation. Instead, *Fibulin-4*$^{R/R}$ aortas show increased ECM remodeling, and increased collagen and elastin structures (Hanada et al., 2007; Moltzer et al., 2011). Yet, they also show increased pSmad2 and pERK activation. A comparison of the Smad3$^{-/-}$ and *Fibulin-4*$^{R/R}$ changes in aneurysm formation is shown in Fig. 8. These findings led us to hypothesize that TGF-β signaling downstream of Smad3 might be deregulated due to Smad3 deficiency.

While AOS and LDS patients have heterozygous loss of function mutations affecting genes from the TGF-β signaling pathway (TGFBR1/2, SMAD3, TGFB2, TGFB3), aortic tissues of these patients show a signature

a

	Smad3 deficiency	Fibulin-4 deficiency
Function	TGFβ signaling	ECM protein
pSmad2	increased	increased
pErk	Increased	increased
Immunosuppression	decreased	present
MMP activity	no change	increased
ECM remodeling	decreased	increased
Aortic stiffness	no change	increased
TGFβ signaling	Activation of TGF-β receptor, no activation of downstream transcriptional response	Activation of TGF-β receptor, and activation of downstream transcriptional response

b

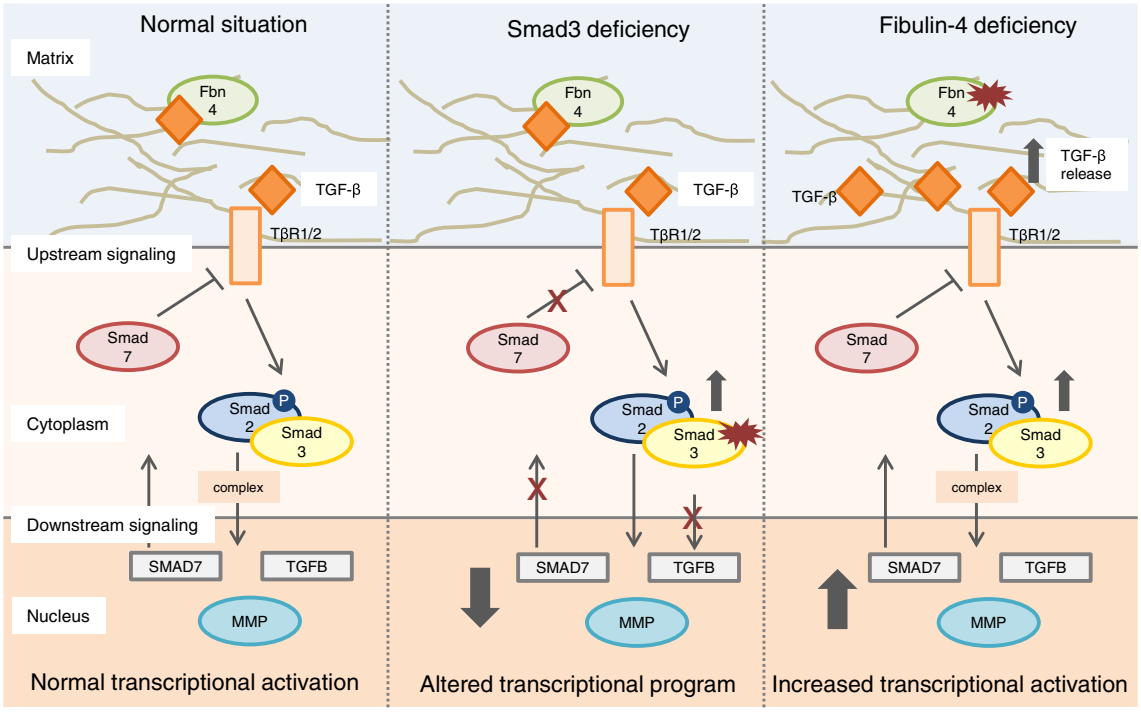

Fig. 8. Comparison of aneurysm formation, and model of differences in TGF-β signaling between *Fibulin-4* and *Smad3* deficient VSMCs. a) Summary of differences between aneurysm formation in *Fibulin-4* and *Smad3* deficient animals. b) Under normal conditions the TGF-β receptor is activated by TGF-β ligand (orange diamond), leading to phosphorylation of Smad2 (pSmad2), which, in complex with Smad3, translocates to the nucleus and induces a transcriptional response (left). One of the genes transcribed is Smad7, a potent inhibitor of upstream TGF-β receptor signaling, thereby providing a regulatory negative feedback loop. In case of Fibulin-4 deficiency, more TGF-β ligand is released from the matrix, leading to increased TGF-β receptor stimulation and Smad2 phosphorylation, resulting in increased downstream transcriptional activation (right). In *Smad3* deficient cells the TGF-β receptor can still be activated by TGF-β ligand, and Smad2 can still be phosphorylated. However, due to absence of Smad3, the Smad2/3 complex will not translocate to the nucleus together, thereby not activating the normal downstream transcriptional program. In case of Smad7 and TGF-β this results in reduced expression. As Smad7 is a potent inhibitor of the TGF-β signaling pathway, when absent or reduced, TGF-β signaling remains activated instead of inhibited. This together could lead to an altered transcriptional program in *Smad3* deficient VSMCs (middle).

of upregulated TGF-β pathway signaling, as indicated by the overexpression of pSMAD2, pERK1/2 and CTGF (Loeys et al., 2005; van de Laar et al., 2011; Lindsay et al., 2012). This phenomenon is known as the TGF-β paradox (for comprehensive review see (Massague, 2012)). We therefore examined TGF-β receptor activation in the aortic wall of *Smad3*$^{-/-}$ animals by investigating pSmad2 expression. We observed that while lacking Smad3, Smad2 can still be phosphorylated and transported to the nucleus. Thus, lack of Smad3 might alter downstream transcriptional activation in the nucleus (also see Fig. 8). This lack of Smad3 might also shift TGF-β activated signaling via Smad2, which has similar but not overlapping functions (Moustakas and Heldin, 2002; Zhang et al., 1996), also resulting in an altered transcriptional response. We reasoned that these changes lead to reduction in the downstream transcription of genes such as ECM components and MMPs. Indeed, we demonstrate here that transcriptional activation of multiple genes downstream of the TGF-β signaling cascade is absent. Again, this is in contrast to what was previously found for *Fibulin-4*$^{R/R}$ aortas and VSMCs where downstream TGF-β-induced transcription was activated (Ramnath et al., 2015). Moreover, we found that the increased proliferation of *Smad3*$^{-/-}$ VSMCs is not due to increased pErk, but rather due to the lack of downstream TGF-β induced transcriptional activation. Moreover, it shows that Smad3 normally plays a role in TGF-β mediated growth inhibition.

We also examined Smad7 as an important regulator of the TGF-β signaling pathway as it inhibits phosphorylation of Smad2 by the TGF-β receptors, thereby acting as a negative feedback loop in this pathway to prevent deregulation. Without Smad7, TGF-β receptor activation cannot be inhibited -explaining for example increased pSmad2- but downstream transcriptional activation remains impaired since Smad3 is lacking (See Fig. 8, left panel for a schematic overview). In agreement, we found no upregulation of Smad7 in *Smad3*$^{-/-}$ aortas, or of other downstream genes such as PAI-1.

When we now compare the findings between *Smad3*$^{-/-}$ and *Fibulin-4*$^{R/R}$ animals, although in both mouse models aneurysms are formed, the underlying cause and phenotypical consequences are quite different (Fig. 8). In *Fibulin-4*$^{R/R}$ aortas it is thought that TGF-β is released from the matrix, resulting in activation of TGF-β signaling pathway, which eventually also results in activated downstream transcription. However, in *Smad3*$^{-/-}$ animals, although there can be activation of TGF-β receptors, as also shown by increased pSmad2 signal, transcriptional activation downstream of Smad3 is impaired. One important downstream gene that is normally transcribed is *SMAD7*, which is a potent inhibitor of the TGF-β signaling pathway. We find decreased *Smad7* transcripts, which might explain the continued activation of the TGF-β receptor. Furthermore, this altered signaling and transcriptional pattern might also lead to an altered 'appearance' of the VSMCs for the immune system, thereby attracting immune cells. In accord, *Smad3*$^{-/-}$ animals suffered from so-called 'sterile' infections in the aortic wall, as derived from the HE stained sections showing infiltrations of immune cells. As these infiltrations were only observed after dilatation of the aorta became apparent, this might suggest that this immune reaction is triggered after the aneurysm is formed. Indeed, Ye et al. showed that administration of anti-GM-CSF antibody to Smad3$^{-/-}$ mice reduced inflammation and also diminished aorta dilation (Ye et al., 2013). This would also be in agreement with the fact that we only observed MMP activity in aortas with an aneurysm that could be traced back to the immune cells adjacent to the adventitia of the aortic wall. Moreover, the fact that here the MMP activation is derived from immune cells rather than from VSMCs, and is only present at late stages of aneurysm formation, after the immune infiltrates are present, would argue that MMP activity is a good marker for aneurysm formation caused by ECM deficiencies, but not for those due to *SMAD3* mutations. The longitudinal echocardiograms showed dilatations with a rapid increase of the aneurysm within a very short period of time. It could be that the increased upstream TGF-β receptor activation, together with the lack of collagen and ECM accumulation results in dilatations; the structural integrity fails progressively. This, together with a possibly altered appearance of the VSMC both in structure as well as transcriptional profile, could attract immune cells, which start cleaning up the detected 'vascular damage' at the expense of macrophage-induced deterioration of the already fragile aortic wall. This would then explain the rapid and aggressive aneurysmal growth.

Most genetic studies have been focusing on delineating the clinical phenotype associated with *SMAD3* mutations (Hilhorst-Hofstee et al., 2013; Aubart et al., 2014; Fitzgerald et al., 2014; Wischmeijer et al., 2013; van der Linde et al., 2012). Despite the increasing number of reported mutations, functional studies indicating the pathological effect of these mutations are lacking. Existing experimental data and molecular predictions suggest that *SMAD3* mutations are mainly loss of function (van de Laar et al., 2011; Aubart et al., 2014). Many reported mutations lead to frame shifts, deletions and likely nonsense mediated decay. Others are perturbing the heterodimer formation SMAD3/4 or leading to nonfunctional complexes. Yet, a dominant-negative effect of some mutations cannot be excluded.

The finding of an aortic phenotype in a mouse model with a complete *Smad3* deficiency very similar to the human disease supports the idea that also lack of functional SMAD3 could cause the human clinical phenotype. A similar scenario has been described for the TGF-β2 mouse model (Boileau et al., 2012). Moreover, in aneurysmal diseases such as Marfan's syndrome (MFS), the efficacy of interventions that target the TGF-β signaling pathway is being explored. So far the effects on delay of aneurysmal growth are quite promising (Neptune et al., 2003; Ng et al., 2004; Habashi et al., 2006; Cohn et al., 2007). However, similar intervention strategies might not be beneficial in case of a *Smad3* deficiency. Since downstream transcriptional activation is hampered in the absence of Smad3, inhibition of components in the TGF-β signaling pathway might in this case worsen the outcome as even less ECM would be generated, and alternative 'escape' pathways would be blocked.

In conclusion, *Smad3* deficiency leads to aortic aneurysms and sudden death in the *Smad3* knockout animal model. This phenotype is influenced by age and gender of the animals. Although Smad3 is absent, we observed increased nuclear translocation of pSmad2, and upregulated pERK signaling, inferring increased upstream TGF-β receptor activation. However, the downstream TGF-β-activated transcriptional response seemed impaired as derived from the absence of MMP activation and lack of amorphous ECM accumulation in *Smad3*$^{-/-}$ mouse aortas. Together our data stress the importance of identifying the molecular mechanism of aneurysmal disease, as the outcome, and therefore treatment options, can differ dramatically. At the same time, the *Smad3*$^{-/-}$ mouse proves to be an ideal model to start testing these different interventional options on.

Supplementary data to this article can be found online at http://dx.doi.org/10.1016/j.ebiom.2016.09.006.

Funding Sources

This study was funded by 'Stichting lijf en leven' (project: dilating versus stenosing arterial disease, 2011–2015), and partially funded by an Erasmus Fellowship (2009) to AM Bertoli-Avella. Funders had no role in study design, data collection, data analysis, interpretation or writing of the manuscript.

Conflicts of Interest

None.

Author contributions

I.P. experimental design, data analysis, figure design, writing of manuscript.

N.V. performed experiments, data analysis, figure design.

J.H.T. data analysis, writing.

J.L.R data analysis, writing.

Y.R. performed experiments, data analysis.

P.M.H. performed experiments, data analysis.
B.S.T. performed experiments, data analysis.
M.V. performed experiments.
R.M.G.B.B.-O. performed experiments.
S.E.H statistical analysis, writing.
H.J.M.V supervision of statistical analysis.
R.K. experimental design, writing.
A.M.B-A. experimental design, writing.
J.E. experimental design, data analysis, writing.

Acknowledgements

We would like to acknowledge Fumiko Itoh, Ph.D. from the Department of Experimental Pathology, University of Tsukuba, Japan, for generous donation of *Smad3* mutant mice.

References

Akhurst, R.J., 2012. The paradoxical TGF-beta vasculopathies. Nat. Genet. 44, 838–839.
Albornoz, G., Coady, M.A., Roberts, M., Davies, R.R., Tranquilli, M., Rizzo, J.A., Elefteriades, J.A., 2006. Familial thoracic aortic aneurysms and dissections—incidence, modes of inheritance, and phenotypic patterns. Ann. Thorac. Surg. 82, 1400–1405.
Aubart, M., Gobert, D., Aubart-Cohen, F., Detaint, D., Hanna, N., D'Indya, H., Lequintrec, J.S., Renard, P., Vigneron, A.M., Dieude, P., Laissy, J.P., Koch, P., Muti, C., Roume, J., Cusin, V., Grandchamp, B., Gouya, L., Leguern, E., Papo, T., Boileau, C., Jondeau, G., 2014. Early-onset osteoarthritis, Charcot-Marie-Tooth like neuropathy, autoimmune features, multiple arterial aneurysms and dissections: an unrecognized and life threatening condition. PLoS One 9, e96387.
Bertoli-Avella, A.M., Gillis, E., Morisaki, H., Verhagen, J.M., de Graaf, B.M., Van de Beek, G., Gallo, E., Kruithof, B.P., Venselaar, H., Myers, L.A., Laga, S., Doyle, A.J., Oswald, G., Van Cappellen, G.W., Yamanaka, I., Van der Helm, R.M., Beverloo, B., de Klein, A., Pardo, L., Lammens, M., Evers, C., Devriendt, K., Dumoulein, M., Timmermans, J., Bruggenwirth, H.T., Verheijen, F., Rodrigus, I., Baynam, G., Kempers, M., Saenen, J., Van Craenenbroeck, E.M., Minatoya, K., Matsukawa, R., Tsukube, T., Kubo, N., Hofstra, R., Goumans, M.J., Bekkers, J.A., Roos-Hesselink, J.W., Van de Laar, I.M., Dietz, H.C., Van Laer, L., Morisaki, T., Wessels, M.W., Loeys, B.L., 2015. Mutations in a TGF-beta ligand, TGFB3, cause syndromic aortic aneurysms and dissections. J. Am. Coll. Cardiol. 65, 1324–1336.
Boileau, C., Guo, D.C., Hanna, N., Regalado, E.S., Detaint, D., Gong, L., Varret, M., Prakash, S.K., Li, A.H., D'Indy, H., Braverman, A.C., Grandchamp, B., Kwartler, C.S., Gouya, L., Santos-Cortez, R.L., Abifadel, M., Leal, S.M., Muti, C., Shendure, J., Gross, M.S., Rieder, M.J., Vahanian, A., Nickerson, D.A., Michel, J.B., National Heart, L., Blood Institute Go Exome Sequencing, P., Jondeau, G., Milewicz, D.M., 2012. TGFB2 mutations cause familial thoracic aortic aneurysms and dissections associated with mild systemic features of Marfan syndrome. Nat. Genet. 44, 916–921.
Chung, A.W., Au Yeung, K., Sandor, G.G., Judge, D.P., Dietz, H.C., Van Breemen, C., 2007. Loss of elastic fiber integrity and reduction of vascular smooth muscle contraction resulting from the upregulated activities of matrix metalloproteinase-2 and −9 in the thoracic aortic aneurysm in Marfan syndrome. Circ. Res. 101, 512–522.
Cohn, R.D., Van Erp, C., Habashi, J.P., Soleimani, A.A., Klein, E.C., Lisi, M.T., Gamradt, M., Ap Rhys, C.M., Holm, T.M., Loeys, B.L., Ramirez, F., Judge, D.P., Ward, C.W., Dietz, H.C., 2007. Angiotensin II type 1 receptor blockade attenuates TGF-beta-induced failure of muscle regeneration in multiple myopathic states. Nat. Med. 13, 204–210.
Dennler, S., Itoh, S., Vivien, D., Ten Dijke, P., Huet, S., Gauthier, J.M., 1998. Direct binding of Smad3 and Smad4 to critical TGF beta-inducible elements in the promoter of human plasminogen activator inhibitor-type 1 gene. EMBO J. 17, 3091–3100.
Fitzgerald, K.K., Bhat, A.M., Conard, K., Hyland, J., Pizarro, C., 2014. Novel SMAD3 mutation in a patient with hypoplastic left heart syndrome with significant aortic aneurysm. Case Rep. Genet. 2014, 591516.
Gillis, E., Van Laer, L., Loeys, B.L., 2013. Genetics of thoracic aortic aneurysm: at the crossroad of transforming growth factor-beta signaling and vascular smooth muscle cell contractility. Circ. Res. 113, 327–340.
Grubb, K.J., Kron, I.L., 2011. Sex and gender in thoracic aortic aneurysms and dissection. Semin. Thorac. Cardiovasc. Surg. 23, 124–125.
Guo, D.C., Pannu, H., Tran-Fadulu, V., Papke, C.L., Yu, R.K., Avidan, N., Bourgeois, S., Estrera, A.L., Safi, H.J., Sparks, E., Amor, D., Ades, L., McConnell, V., Willoughby, C.E., Abuelo, D., Willing, M., Lewis, R.A., Kim, D.H., Scherer, S., Tung, P.P., Ahn, C., Buja, L.M., Raman, C.S., Shete, S.S., Milewicz, D.M., 2007. Mutations in smooth muscle alpha-actin (ACTA2) lead to thoracic aortic aneurysms and dissections. Nat. Genet. 39, 1488–1493.
Habashi, J.P., Judge, D.P., Holm, T.M., Cohn, R.D., Loeys, B.L., Cooper, T.K., Myers, L., Klein, E.C., Liu, G., Calvi, C., Podowski, M., Neptune, E.R., Halushka, M.K., Bedja, D., Gabrielson, K., Rifkin, D.B., Carta, L., Ramirez, F., Huso, D.L., Dietz, H.C., 2006. Losartan, an AT1 antagonist, prevents aortic aneurysm in a mouse model of Marfan syndrome. Science 312, 117–121.
Hanada, K., Vermeij, M., Garinis, G.A., de Waard, M.C., Kunen, M.G., Myers, L., Maas, A., Duncker, D.J., Meijers, C., Dietz, H.C., Kanaar, R., Essers, J., 2007. Perturbations of vascular homeostasis and aortic valve abnormalities in fibulin-4 deficient mice. Circ. Res. 100, 738–746.
Hawinkels, L.J., Paauwe, M., Verspaget, H.W., Wiercinska, E., Van der Zon, J.M., Van der Ploeg, K., Koelink, P.J., Lindeman, J.H., Mesker, W., Ten Dijke, P., Sier, C.F., 2014. Interaction with colon cancer cells hyperactivates TGF-beta signaling in cancer-associated fibroblasts. Oncogene 33, 97–107.
Hilhorst-Hofstee, Y., Scholte, A.J., Rijlaarsdam, M.E., Van Haeringen, A., Kroft, L.J., Reijnierse, M., Ruivenkamp, C.A., Versteegh, M.I., Pals, G., Breuning, M.H., 2013. An unanticipated copy number variant of chromosome 15 disrupting SMAD3 reveals a three-generation family at serious risk for aortic dissection. Clin. Genet. 83, 337–344.
Huang, J., Davis, E.C., Chapman, S.L., Budatha, M., Marmorstein, L.Y., Word, R.A., Yanagisawa, H., 2010. Fibulin-4 deficiency results in ascending aortic aneurysms: a potential link between abnormal smooth muscle cell phenotype and aneurysm progression. Circ. Res. 106, 583–592.
Kaijzel, E.L., Van Heijningen, P.M., Wielopolski, P.A., Vermeij, M., Koning, G.A., Van Cappellen, W.A., Que, I., Chan, A., Dijkstra, J., Ramnath, N.W., Hawinkels, L.J., Bernsen, M.R., Lowik, C.W., Essers, J., 2010. Multimodality imaging reveals a gradual increase in matrix metalloproteinase activity at aneurysmal lesions in live fibulin-4 mice. Circ. Cardiovasc. Imaging 3, 567–577.
Lemaitre, V., Soloway, P.D., D'Armiento, J., 2003. Increased medial degradation with pseudo-aneurysm formation in apolipoprotein E-knockout mice deficient in tissue inhibitor of metalloproteinases-1. Circulation 107, 333–338.
Li, T.F., Darowish, M., Zuscik, M.J., Chen, D., Schwarz, E.M., Rosier, R.N., Drissi, H., O'Keefe, R.J., 2006. Smad3-deficient chondrocytes have enhanced BMP signaling and accelerated differentiation. J. Bone Miner. Res. 21, 4–16.
Li, C.G., Liang, Q.Q., Zhou, Q., Menga, E., Cui, X.J., Shu, B., Zhou, C.J., Shi, Q., Wang, Y.J., 2009. A continuous observation of the degenerative process in the intervertebral disc of Smad3 gene knock-out mice. Spine (Phila Pa 1976) 34, 1363–1369.
Lindsay, M.E., Dietz, H.C., 2011. Lessons on the pathogenesis of aneurysm from heritable conditions. Nature 473, 308–316.
Lindsay, M.E., Schepers, D., Bolar, N.A., Doyle, J.J., Gallo, E., Fert-Bober, J., Kempers, M.J., Fishman, E.K., Chen, Y., Myers, L., Bjeda, D., Oswald, G., Elias, A.F., Levy, H.P., Anderlid, B.M., Yang, M.H., Bongers, E.M., Timmermans, J., Braverman, A.C., Canham, N., Mortier, G.R., Brunner, H.G., Byers, P.H., Van Eyk, J., Van Laer, L., Dietz, H.C., Loeys, B.L., 2012. Loss-of-function mutations in TGFB2 cause a syndromic presentation of thoracic aortic aneurysm. Nat. Genet. 44, 922–927.
Loeys, B.L., Chen, J., Neptune, E.R., Judge, D.P., Podowski, M., Holm, T., Meyers, J., Leitch, C.C., Katsanis, N., Sharifi, N., Xu, F.L., Myers, L.A., Spevak, P.J., Cameron, D.E., de Backer, J., Hellemans, J., Chen, Y., Davis, E.C., Webb, C.L., Kress, W., Coucke, P., Rifkin, D.B., de Paepe, A.M., Dietz, H.C., 2005. A syndrome of altered cardiovascular, craniofacial, neurocognitive and skeletal development caused by mutations in TGFBR1 or TGFBR2. Nat. Genet. 37, 275–281.
Longo, G.M., Xiong, W., Greiner, T.C., Zhao, Y., Fiotti, N., Baxter, B.T., 2002. Matrix metalloproteinases 2 and 9 work in concert to produce aortic aneurysms. J. Clin. Invest. 110, 625–632.
Martens, T., Van Herzeele, I., de Ryck, F., renard, M., de Paepe, A., Francois, K., Vermassen, F., de Backer, J., 2013. Multiple aneurysms in a patient with aneurysms-osteoarthritis syndrome. Ann. Thorac. Surg. 95, 332–335.
Massague, J., 2012. TGFbeta signalling in context. Nat. Rev. Mol. Cell Biol. 13, 616–630.
Massague, J., Seoane, J., Wotton, D., 2005. Smad transcription factors. Genes Dev. 19, 2783–2810.
McAllister, K.A., Grogg, K.M., Johnson, D.W., Gallione, C.J., Baldwin, M.A., Jackson, C.E., Helmbold, E.A., Markel, D.S., McKinnon, W.C., Murrell, J., et al., 1994. Endoglin, a TGF-beta binding protein of endothelial cells, is the gene for hereditary haemorrhagic telangiectasia type 1. Nat. Genet. 8, 345–351.
McLaughlin, P.J., Chen, Q., Horiguchi, M., Starcher, B.C., Stanton, J.B., Broekelmann, T.J., Marmorstein, A.D., McKay, B., Mecham, R., Nakamura, T., Marmorstein, L.Y., 2006. Targeted disruption of fibulin-4 abolishes elastogenesis and causes perinatal lethality in mice. Mol. Cell. Biol. 26, 1700–1709.
Mizuguchi, T., Collod-Beroud, G., Akiyama, T., Abifadel, M., Harada, N., Morisaki, T., Allard, D., Varret, M., Claustres, M., Morisaki, H., Ihara, M., Kinoshita, A., Yoshiura, K., Junien, C., Kajii, T., Jondeau, G., Ohta, T., Kishino, T., Furukawa, Y., Nakamura, Y., Niikawa, N., Boileau, C., Matsumoto, N., 2004. Heterozygous TGFBR2 mutations in Marfan syndrome. Nat. Genet. 36, 855–860.
Moltzer, E., Te Riet, L., Swagemakers, S.M., Van Heijningen, P.M., Vermeij, M., Van Veghel, R., Bouhuizen, A.M., Van Esch, J.H., Lankhorst, S., Ramnath, N.W., de Waard, M.C., Duncker, D.J., Van der Spek, P.J., Rouwet, E.V., Danser, A.H., Essers, J., 2011. Impaired vascular contractility and aortic wall degeneration in fibulin-4 deficient mice: effect of angiotensin II type 1 (AT1) receptor blockade. PLoS One 6, e23411.
Moustakas, A., Heldin, C.H., 2002. From mono- to oligo-Smads: the heart of the matter in TGF-beta signal transduction. Genes Dev. 16, 1867–1871.
Nahrendorf, M., Keliher, E., Marinelli, B., Leuschner, F., Robbins, C.S., Gerszten, R.E., Pittet, M.J., Swirski, F.K., Weissleder, R., 2011. Detection of macrophages in aortic aneurysms by nanoparticle positron emission tomography-computed tomography. Arterioscler. Thromb. Vasc. Biol. 31, 750–757.
Neptune, E.R., Frischmeyer, P.A., Arking, D.E., Myers, L., Bunton, T.E., Gayraud, B., Ramirez, F., Sakai, L.Y., Dietz, H.C., 2003. Dysregulation of TGF-beta activation contributes to pathogenesis in Marfan syndrome. Nat. Genet. 33, 407–411.
Ng, C.M., Cheng, A., Myers, L.A., Martinez-Murillo, F., Jie, C., Bedja, D., Gabrielson, K.L., Hausladen, J.M., Mecham, R.P., Judge, D.P., Dietz, H.C., 2004. TGF-beta-dependent pathogenesis of mitral valve prolapse in a mouse model of Marfan syndrome. J. Clin. Invest. 114, 1586–1592.
Ramnath, N.W., Hawinkels, L.J., Van Heijningen, P.M., Riet, L.T., Paauwe, M., Vermeij, M., Danser, A.H., Kanaar, R., Ten Dijke, P., Essers, J., 2015. Fibulin-4 deficiency increases TGF-beta signalling in aortic smooth muscle cells due to elevated TGF-beta2 levels. Sci. Rep. 5, 16872.
Regalado, E.S., Guo, D.C., Villamizar, C., Avidan, N., Gilchrist, D., McGillivray, B., Clarke, L., Bernier, F., Santos-Cortez, R.L., Leal, S.M., Bertoli-Avella, A.M., Shendure, J., Rieder, M.J., Nickerson, D.A., Project, N. G. E. S., Milewicz, D.M., 2011. Exome sequencing

identifies SMAD3 mutations as a cause of familial thoracic aortic aneurysm and dissection with intracranial and other arterial aneurysms. Circ. Res. 109, 680–686.

Renard, M., Holm, T., Veith, R., Callewaert, B.L., Ades, L.C., Baspinar, O., Pickart, A., Dasouki, M., Hoyer, J., Rauch, A., Trapane, P., Earing, M.G., Coucke, P.J., Sakai, L.Y., Dietz, H.C., de Paepe, A.M., Loeys, B.L., 2010. Altered TGFbeta signaling and cardiovascular manifestations in patients with autosomal recessive cutis laxa type I caused by fibulin-4 deficiency. Eur. J. Hum. Genet. 18, 895–901.

Renard, M., Callewaert, B., Baetens, M., Campens, L., MacDermot, K., Fryns, J.P., Bonduelle, M., Dietz, H.C., Gaspar, I.M., Cavaco, D., Stattin, E.L., Schrander-Stumpel, C., Coucke, P., Loeys, B., de Paepe, A., de Backer, J., 2013. Novel MYH11 and ACTA2 mutations reveal a role for enhanced TGFbeta signaling in FTAAD. Int. J. Cardiol. 165, 314–321.

Rienhoff, H.Y.J., Yeo, C.Y., Morissette, R., Khrebtukova, I., Melnick, J., Luo, S., Leng, N., Kim, Y.J., Schroth, G., Westwick, J., Vogel, H., McDonnell, N., Hall, J.G., Whitman, M., 2013. A mutation in TGFB3 associated with a syndrome of low muscle mass, growth retardation, distal arthrogryposis and clinical features overlapping with Marfan and Loeys-Dietz syndrome. Am. J. Med. Genet. A 161A, 2040–2046.

Segura, A.M., Luna, R.E., Horiba, K., Stetler-Stevenson, W.G., Mcallister Jr., H.A., Willerson, J.T., Ferrans, V.J., 1998. Immunohistochemistry of matrix metalloproteinases and their inhibitors in thoracic aortic aneurysms and aortic valves of patients with Marfan's syndrome. Circulation 98, II331–II337 discussion II337–8.

Te Riet, L., Van Deel, E.D., Van Thiel, B.S., Moltzer, E., Van Vliet, N., Ridwan, Y., Van Veghel, R., Van Heijningen, P.M., Robertus, J.L., Garrelds, I.M., Vermeij, M., Van der Pluijm, I., Danser, A.H., Essers, J., 2016. AT1-receptor blockade, but not renin inhibition, reduces aneurysm growth and cardiac failure in fibulin-4 mice. J. Hypertens. 34, 654–665.

Van de Laar, I.M., Oldenburg, R.A., Pals, G., Roos-Hesselink, J.W., de Graaf, B.M., Verhagen, J.M., Hoedemaekers, Y.M., Willemsen, R., Severijnen, L.A., Venselaar, H., Vriend, G., Pattynama, P.M., Collee, M., Majoor-Krakauer, D., Poldermans, D., Frohn-Mulder, I.M., Micha, D., Timmermans, J., Hilhorst-Hofstee, Y., Bierma-Zeinstra, S.M., Willems, P.J., Kros, J.M., Oei, E.H., Oostra, B.A., Wessels, M.W., Bertoli-Avella, A.M., 2011. Mutations in SMAD3 cause a syndromic form of aortic aneurysms and dissections with early-onset osteoarthritis. Nat. Genet. 43, 121–126.

Van de Laar, I.M., Van der Linde, D., Oei, E.H., Bos, P.K., Bessems, J.H., Bierma-Zeinstra, S.M., Van Meer, B.L., Pals, G., Oldenburg, R.A., Bekkers, J.A., Moelker, A., de Graaf, B.M., Matyas, G., Frohn-Mulder, I.M., Timmermans, J., Hilhorst-Hofstee, Y., Cobben, J.M., Bruggenwirth, H.T., Van Laer, L., Loeys, B., de Backer, J., Coucke, P.J., Dietz, H.C., Willems, P.J., Oostra, B.A., de Paepe, A., Roos-Hesselink, J.W., Bertoli-Avella, A.M., Wessels, M.W., 2012. Phenotypic spectrum of the SMAD3-related aneurysms-osteoarthritis syndrome. J. Med. Genet. 49, 47–57.

Van der Linde, D., Van de Laar, I.M., Bertoli-Avella, A.M., Oldenburg, R.A., Bekkers, J.A., Mattace-Raso, F.U., Van den Meiracker, A.H., Moelker, A., Van Kooten, F., Frohn-Mulder, I.M., Timmermans, J., Moltzer, E., Cobben, J.M., Van Laer, L., Loeys, B., de Backer, J., Coucke, P.J., de Paepe, A., Hilhorst-Hofstee, Y., Wessels, M.W., Roos-Hesselink, J.W., 2012. Aggressive cardiovascular phenotype of aneurysms-osteoarthritis syndrome caused by pathogenic SMAD3 variants. J. Am. Coll. Cardiol. 60, 397–403.

Van der Linde, D., Van de Laar, I., Moelker, A., Wessels, M.W., Bertoli-Avella, A.M., Roos-Hesselink, J.W., 2013. Patients with aneurysms and osteoarthritis: Marfan syndrome ruled out, so what is it?] Patienten met aneurysmata en osteoartritis: geen syndroom van Marfan, maar wat dan? Ned. Tijdschr. Geneeskd. 157, A5588.

Wischmeijer, A., Van Laer, L., Tortora, G., Bolar, N.A., Van Camp, G., Fransen, E., Peeters, N., Di Bartolomeo, R., Pacini, D., Gargiulo, G., Turci, S., Bonvicini, M., Mariucci, E., Lovato, L., Brusori, S., Ritelli, M., Colombi, M., Garavelli, L., Seri, M., Loeys, B.L., 2013. Thoracic aortic aneurysm in infancy in aneurysms-osteoarthritis syndrome due to a novel SMAD3 mutation: further delineation of the phenotype. Am. J. Med. Genet. A 161A, 1028–1035.

Yang, X., Cao, X., 2001. Smad interactors in bone morphogenetic protein signaling. Methods Mol. Biol. 177, 163–178.

Ye, P., Chen, W., Wu, J., Huang, X., Li, J., Wang, S., Liu, Z., Wang, G., Yang, X., Zhang, P., Lv, Q., Xia, J., 2013. GM-CSF contributes to aortic aneurysms resulting from SMAD3 deficiency. J. Clin. Invest. 123, 2317–2331.

Zhang, Y., Feng, X., We, R., Derynck, R., 1996. Receptor-associated Mad homologues synergize as effectors of the TGF-beta response. Nature 383, 168–172.

Zhu, L., Vranckx, R., Khau Van Kien, P., Lalande, A., Boisset, N., Mathieu, F., Wegman, M., Glancy, L., Gasc, J.M., Brunotte, F., Bruneval, P., Wolf, J.E., Michel, J.B., Jeunemaitre, X., 2006. Mutations in myosin heavy chain 11 cause a syndrome associating thoracic aortic aneurysm/aortic dissection and patent ductus arteriosus. Nat. Genet. 38, 343–349.